Andean Geology 50 (3): 319-345. September, 2023 doi: 10.5027/andgeoV50n3-3650

# The April 2015 Calbuco eruption pyroclastic density currents: deposition, impacts on woody vegetation, and cooling on the northern flank of the cone

\*Jorge E. Romero<sup>1</sup>, Frederick J. Swanson<sup>2</sup>, Julia A. Jones<sup>3</sup>, Daniele Morgavi<sup>4</sup>, Guido Giordano<sup>5</sup>, Matteo Trolese<sup>6</sup>, Felipe Aguilera<sup>7,8</sup>, Tatiana Izquierdo<sup>9</sup>, Diego Perugini<sup>10</sup>

- <sup>1</sup> Instituto de Ciencias de la Ingeniería, Universidad de O'Higgins, Libertador Bernardo O'Higgins 611, Rancagua, Chile. jorge.romero@uoh.cl
- <sup>2</sup> Pacific Northwest Research Station, U.S. Forest Service, Corvallis, Oregon, 1220 SW 3rd Ave. Suite 1400, Portland, OR 97204, United States. fjswanson541@gmail.com
- <sup>3</sup> College of Earth, Ocean, and Atmospheric Sciences, Oregon State University, Corvallis, 1500 SW Jefferson Way, OR 97331, United States. julia.jones@oregonstate.edu
- Dipartimento di Scienze della Terra, dell'Ambiente e delle Risorse, Università degli Studi di Napoli Federico II, Largo S. Marcellino 10, 80138 Napoli NA, Italy.
  - daniele.morgavi@unina.it
- <sup>5</sup> Dipartimento di Scienze, Sezione di Geologia, Università degli Studi Roma Tre, Viale Guglielmo Marconi, 446, Rome, Italy. guido.giordano@uniroma3.it
- <sup>6</sup> Jackson School of Geosciences, The University of Texas, 2305 Speedway, Stop C1160, Austin, TX 78712-1692, United States. matteo.trolese@jsg.utexas.edu
- <sup>7</sup> Instituto Milenio de Investigación en Riesgo Volcánico-Ckelar Volcanes, Avda. Angamos 0610, Antofagasta, Chile.
- 8 Departamento de Ciencias Geológicas, Universidad Católica del Norte, Avda. Angamos 0610, Antofagasta, Chile. feaguilera@ucn.cl
- 9 Departamento de Biología y Geología, Física y Química Inorgánica, Universidad Rey Juan Carlos, Calle Tulipán, s/n 28933 Móstoles, Spain.
  - tatiana.izquierdo@urjc.es
- Deptartment of Physics and Geology, University of Perugia, Piazza dell'Università, 06123, Perugia, Italy. diego.perugini@unipg.it
- \* Corresponding author: jorge.romero@uoh.cl

ABSTRACT. The 22-23 April 2015 eruption of the Calbuco volcano (Southern Andes, Chile) led to extensive pyroclastic density currents (PDCs) interactions with vegetation. We seek to describe the PDCs which affected both Tepu and Frío rivers, northern Calbuco, from their timing and deposition to cooling and erosion, as well as their impacts on forests. Our investigation is based on field stratigraphy, forest disturbance assessment, and geothermometry from degassing pipes and charcoal. These PDCs reached at least ~540-603 °C, as estimated from fumaroles, and consisted of both concentrated and dilute PDCs during the first pulse (22 April) at Tepu and mainly during the second pulse (23 April) at Frío. Effects of PDCs on forest vegetation recorded in Tepu consisted of heating, abrasion, burial, and impact force. On the valley floor, trees were buried with up to 4 m of deposits from the concentrated PDCs, and all trees in this deposition zone died with no subsequent sprouting. Conversely, in the margins of the valley, defoliated fallen trees and standing shrubs indicate scorching due to the passage of dilute PDCs, and some of them were later sprouting. Estimated impact forces required to produce toppling range from 1.5 to 3.7 kPa, and PDC velocities reached up to 36 m s<sup>-1</sup>. Charring of the buried wood involved an emplacement temperature of 400-550 °C within PDC deposits. The rapid watershed formation may have

facilitated infiltration, decreasing the temperature in the basal part within the deposits at the Tepu river. Runoff during the subsequent months triggered lahars and caused the rivers to incise the deposits and transport sediment downstream. This set of observations provides valuable insights into how the interaction between volcanic phenomena and margine forest on the valley floors informs eruptive processes, dynamics, and impacts. Our study is also relevant to interpret the thermal history and potential hazards of PDCs.

Keywords: Calbuco volcano, Volcaniclastic deposits, Ecological disturbance, Dynamic pressure, Flow velocity, Geothermometry.

RESUMEN. Las corrientes de densidad piroclástica de la erupción del volcán Calbuco en abril de 2015: depositación, impactos sobre la vegetación leñosa y enfriamiento en el flanco norte del cono. La erupción del volcán Calbuco (Andes del Sur, Chile), entre el 22 y 23 de abril de 2015, provocó extensas interacciones entre las corrientes piroclásticas de densidad (CDP) con la vegetación. En este trabajo se describen las CDP que afectaron a los ríos Tepu y Frío, al norte del Calbuco, desde su cronología y depositación hasta su enfriamiento y erosión, así como su impacto en los bosques. Nuestra investigación se basa en la estratigrafía de campo, la evaluación de la perturbación forestal y la geotermometría a partir de pipas de desgasificación y carbón vegetal. Estas CDP alcanzaron al menos ~540-603 °C, según las estimaciones de las fumarolas, y consistieron tanto en corrientes concentradas como diluidas durante el primer pulso (22 de abril) en el Tepu y principalmente durante el segundo pulso (23 de abril) en el Frío. Los efectos de las CDP en la vegetación forestal registrados en el Tepu consistieron en calentamiento, abrasión, enterramiento y fuerza de impacto. En el fondo del valle, los árboles quedaron enterrados incluso bajo 4 m de depósitos de CDP concentradas, y todos murieron sin brotar. Por el contrario, en los márgenes del valle, los árboles caídos defoliados y los arbustos en pie indican quemaduras debidas al paso de CDP diluidas, y algunos de ellos brotaron. Las fuerzas de impacto estimadas necesarias para derribar los árboles oscilan entre 1,5 y 3,7 kPa, y las velocidades de las CDP alcanzaron hasta 36 m s<sup>-1</sup>. La carbonización de la madera enterrada supuso una temperatura de emplazamiento de 400-550 °C dentro de los depósitos de CDP. La rápida formación de drenajes puede haber facilitado la infiltración, disminuyendo la temperatura en la parte basal de los depósitos en el río Tepu. La escorrentía durante los meses posteriores desencadenó lahares secundarios y provocó que los ríos incidieran en los depósitos y transportaran sedimentos río abajo. Este conjunto de observaciones proporciona valiosos conocimientos sobre la interacción entre los fenómenos volcánicos y el bosque ribereño en los fondos de valle, la cual es importante para comprender los procesos, la dinámica y los impactos de la erupción. Nuestro estudio también es relevante para interpretar la historia térmica y los peligros potenciales de las CDP.

Palabras clave: Volcán Calbuco, Depósitos volcanoclásticos, Perturbación ecológica, Presión dinámica, Velocidad de flujo, Geotermometría.

#### 1. Introduction

Pyroclastic density currents (PDCs) are hazardous volcanic processes, threatening human populations around volcanoes due to their rapid propagation along the ground, large dynamic pressures, and high temperatures. PDCs are particle-laden, gravity currents transporting fresh lava fragments, hot gases, and non-juvenile lithic clasts of varying origin, size, and density (Branney and Kokelaar, 2002). Generation mechanisms include transient events, such as partial column collapse, dome collapse, dome explosions and lateral blasts, or long-term phenomena, such as continuous column collapse and boiling over events (Sulpizio et al., 2014). PDCs commonly leave deposits in valleys and gullies on the flanks of the volcano, altering landforms and disturbing ecological systems. Collectively, PDCs processes may be reflected in damage to vegetation by the mechanisms of heating, impact force, burial, and abrasion. Posteruptive processes involving water (e.g., lahars) add complexity to the fresh landscapes initially created by PDCs and tephra fall (Vallance and Iverson, 2015). Therefore, many of the evidence of forest impact will be lost to erosion, wood decomposition, deposit cooling, etc.

The frequent eruptions and extensive forests of the Southern Andes volcanoes provide excellent opportunities for the study of interactions among eruptive processes, hydrogeomorphic processes, and forest vegetation (*e.g.*, Pierson *et al.*, 2013; Swanson *et al.*, 2013; Major *et al.*, 2016; Swanson *et al.*, 2016). In this respect, the 22-23 April 2015 Calbuco volcano eruption (41°20' S-72°37' W, Southern Andes) has been investigated in detail regarding its products and dynamics (*e.g.*, Castruccio *et al.*, 2016; Reckziegel *et al.*, 2016; Romero *et al.*, 2019; Morgado *et al.*, 2019; Romero *et al.*, 2021). However, less attention has been paid to the 2015 PDCs and the

subsequent hydrogeomorphic processes (*e.g.*, Mella *et al.*, 2015; Jones, 2016; Macorps, 2021; Zingaretti *et al.*, 2023) and no reports are available on their interactions with forests to our best knowledge.

Studying deposition, interaction with forest, cooling, and erosion of the 2015 Calbuco PDCs provides clues on PDC dynamic properties, direct impacts and reorganization of sediment and organic matter (e.g., Major et al., 2013, 2016). Moreover, large wood may increase the hazards posed by posteruption floods, the effect of surviving organic matter in soil and ecosystem responses to eruptions, and the contribution of wood to carbon dynamics (e.g., Swanson et al., 2021). In this paper, we examine the effects of the Calbuco eruption on near-by watersheds, showing the characteristics of the PDC and lahar deposits on the valley floors of the Tepu and Frío rivers (a tributary to Blanco-Este River) in channels draining the northeast flank of Calbuco (Fig. 1A, B). Rainfall did not occur during the eruption nor for several weeks afterward. Therefore, this study is able to examine effects caused purely by PDCs without immediate alteration by lahars or fluvial erosion. We provide fresh descriptions of PDC stratigraphy, forest disturbance, timing of deposit cooling and erosion, and geothermometry from degassing pipes and charcoal. This evidence is used to constrain the timing, movement, deposition dynamics, impact mechanisms, cooling, and erosion of these PDCs and their deposits. This multidisciplinary approach provides valuable information on the dynamics and hazard of PDCs, as well as their role in modifying both the ecosystem and the landscape of active volcanoes. These elements also contribute to volcanic geoheritage and volcanic hazard management, as shown in the companion paper of Sánchez et al. (in prep.)<sup>1</sup>. Our study also complements the volcano ecology research focused on tephra fall in Valdivian rainforess (e.g., Swanson et al., 2013, 2016; Hintz et al., 2021).

# 1.1. Calbuco volcano, its environment, and the 2015 eruption

Calbuco is an active stratovolcano (2,015 m a.s.l.) in the Southern Andes of Chile with at least 37 eruptions between 8460 BCE and 2014 (Global Volcanism Program, 2013). At least five sub-Plinian and several small- to moderate-Vulcanian eruptions have occurred in the past 125 years, producing lava

flows, tephra fallout, PDCs and lahars down major river channels draining in all directions from the volcano, but especially those draining to the north (e.g., Stone, 1930<sup>2</sup>; Klohn, 1963; Moreno et al., 2006; Castruccio et al., 2010; Sellés and Moreno, 2011; Romero et al., 2021).

Calbuco lies in a temperate climate classified as Marine West Coast (Sarricolea et al., 2017) determined by the relatively low elevation of the Andes, the influence of westerly winds, high rainfall and oceanic conditions. The mean annual rainfall in Puerto Montt (32 km SW from Calbuco) is 1,756 mm (Bown, 2004). From January to March, mean monthly rainfall is less than 100 mm, whereas from May to August it exceeds 200 mm (Valdés-Pineda et al., 2014). In addition, the volcano is typically snow covered above 900 m a.s.l. during the winter (DGA, 1995). Steep drainages from the volcano result from the proximity to base level at Llanquihue Lake (70 m a.s.l.). Tepu River (~20 km² total catchment area) has a mean slope of 18% along its 10.5 km length, while the mean slope of the Frío and Blanco-Este rivers (~40 km<sup>2</sup> catchment area) is 13% along 14.9 km, leading them to have high capacity for erosion and sediment transport. Before the April 2015 eruption, channel width ranged from 3 to 7 m in the Tepu study area and from 4 to 5 m in the Frío study area.

Before the 2015 eruption, vegetation above 500 m a.s.l. on the northeast flank was native, evergreen, broadleaf Valdivian rainforest, including Nothofagus dombeyi with individuals predating 1727 CE (Hernández, 2018). Secondary forest and non-forest vegetation occupied lower elevations, reflecting a history of logging, farming, and pasturing. The older trees survived many tephra falls and PDC events over the previous several centuries (Romero *et al.*, 2021). Vegetation on the valley floors of Tepu and Frío rivers was generally small trees (<20 cm diameter at breast height, DBH, measured at 137 cm above the ground), including Eucryphia cordifolia and Caldcluvia paniculata, which eventually established after passage of PDCs and lahars associated with the 1961 eruption (e.g., Klohn, 1963). However, large, old trees of species such as Laureliopsis philippianna and Caldcluvia paniculata occurred at low density on higher terraces along the valley floor above the zone of flow deposits and on the adjacent, steep valley walls.

The 22-23 April 2015, eruption of Calbuco was an extension of this historic activity in both

<sup>&</sup>lt;sup>1</sup> Sánchez, F.; Romero, J.E.; Pereira, P.; Schilling, M. (in prep.). Geosites assessment in the northern flank of Calbuco volcano (Southern Andes, Chile).

<sup>&</sup>lt;sup>2</sup> Stone, J. 1930. Two active volcanoes of Chile. The Volcano Letter 284. Hawaiian Volcano Observatory: 284 p. Hawaii.

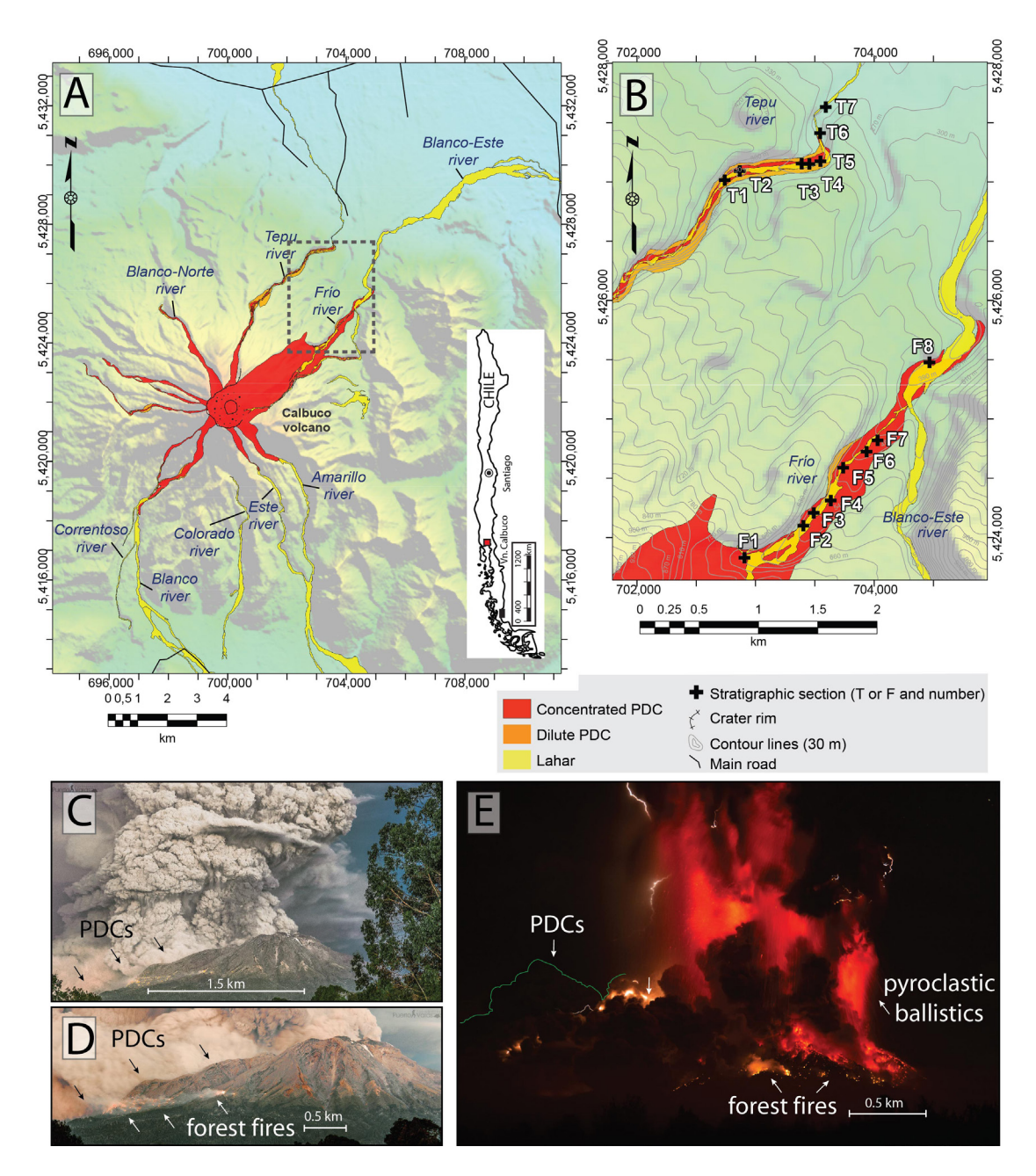


FIG. 1. A. Map of PDC and lahar deposits of the 2015 eruption of Calbuco volcano (after Mella *et al.*, 2015). **B.** Location of stratigraphic stations. C-E. Correspond to photographs of the 1<sup>st</sup> (C and D) and 2<sup>nd</sup> (E) eruptive pulses on 22 and 23 April 2015, respectively, as seen from the NW (Credits: A. Becerra and G. Cifuentes).

magnitude and volcanic products (Mella *et al.*, 2015; Castruccio *et al.*, 2016; Jones, 2016; Romero *et al.*, 2016, 2021). The eruption initiated with short-lived (<3 h) geophysical precursors (Arzilli *et al.*, 2019; Morgado *et al.*, 2019) producing three different pulses

with columns of 15, 17, and 5 km high on 22, 23, and 30 April 2015. The overall eruption was sub-Plinian and erupted ~0.28-0.58 km<sup>3</sup> of bulk tephra to the northeast of the cone, even to Argentina and around the globe (Bertin *et al.*, 2015; Castruccio *et al.*,

2016; Reckziegel et al., 2016; Romero et al., 2016, 2021). Small column collapses were directly observed occurring north from Calbuco during the first pulse (Fig. 1C; Castruccio et al., 2016) Simultaneously, several forest fires were triggered by the fallout of pyroclastic bombs on forest or by lightning strikes (Fig. 1D) generated by charge within the column and low-level co-PDC ash plumes (Fig. 1E; Van Eaton et al., 2016). PDC deposits covered the upper reaches of the valley floors of several river valleys draining radially from the volcano (Fig. 1A). The bulk volume of PDCs has been estimated at 0.01-0.07 km<sup>3</sup>, attaining run out distances of 7-8 km down the Blanco-Este and Frío Rivers (Mella et al., 2015; Castruccio et al., 2016; Van Eaton et al., 2016) and 7.5 km down the Tepu River. Particularly at Blanco-Este and Frío Rivers, the PDC volume was estimated to  $5.2\pm1.3\times10^6$  m<sup>3</sup> by Macorps (2021).

#### 2. Materials and methods

# 2.1. Precipitation records, runoff estimation and geomorphologic analysis

The 2001-2010 monthly precipitation records for the Ensenada, Puerto Montt and Puelo rainfall gauges (Water Resources Directorate, DGA; Web page: www.dga.cl) show an inverse correlation between elevation and precipitation. Although none of these gauges are located inside our study area, their geographic distribution makes them representative of the amount of precipitation that falls in the study sites. The Ensenada gauge (10 km northeast of the summit) was not active in 2015, so we use records from nearby sites that include the immediate preand post-eruption period. Observations of the pace of fluvial erosion were made by field visits, Google Earth and drone images, and reports and photographs from local residents.

# 2.2. Analysis of the PDCs and lahars in valleys of Tepu and Frío rivers

We conducted six field campaigns in the Tepu and Frío valleys between May 2015 and December 2019 (Fig. 1B). During visits in 2016-2018, we observed profiles in stream cuts in the new deposits, and very limited exposures of pre-eruption stream bed and banks and floodplain areas where fluvial erosion had removed a large fraction of the 2015 deposits. Fifteen

stratigraphic columns of PDC deposits were drawn and correlated following lithologic and stratigraphic relationships (Fig. 2). These observations substantially add to the published works of Mella *et al.* (2015) and Castruccio *et al.* (2016). Interpretation of dilute PDCs in these valleys was based on observations of scorched (standing dead trees) and toppled (fallen in a down-valley direction) vegetation on the hillsides along sections of Tepu River and several thin (few cm thick) ash deposits observed within and at the base of PDC deposit profiles exposed by fluvial erosion of the PDC valley fill.

# 2.3. Vegetation and observations of damage

We examined vegetation in the two valleys to determine effects of PDCs on vegetation (e.g., removal, tipping, charring) so that we could use that information to interpret properties of the PDC processes and deposits and selected consequences of PDC-vegetation interactions. We interpreted preeruption vegetation on the valley floors of the Tepu and Frío rivers from Google Earth images (9 March 2012, 10 January 2014), eyewitness accounts, and inspection of remnants of vegetation exposed by fluvial erosion of the fresh PDC and lahar deposits. To characterize surviving and damaged vegetation, we installed plots (Plot A=T2, Plot B=T3, Plot C=T6 in Fig. 1B) comprised of line transects 6 m wide and 50 m long in Jan 2018 in three areas of the Tepu valley floor where fluvial erosion had exposed the pre-eruption valley floor soil surface and remnant trees (Fig. 3). Plot D (1 km downstream of T7 in Fig. 1B), considered a control plot, it was downstream of the toe of the PDC deposits and did not experience disturbance to the valley floor vegetation during the

No pre-eruption remnants of forest were exposed in the valley floor of Frío, so we did not install similar plots there. In both sites, we sought evidence of impact force by PDCs and lahars that had been sufficient to remove trees rather than simply tip them over, such as pits where trees were uprooted, or entire trees with root systems embedded in PDC deposits.

The features of the dead forest stems (diameter, length, orientation [vertical, tipped, curved], and degree of charring) were characterized at each plot. We measured DBH for all standing trees with basal diameter greater than or equal to 5 cm and taller than breast height. For shorter tree stems meeting

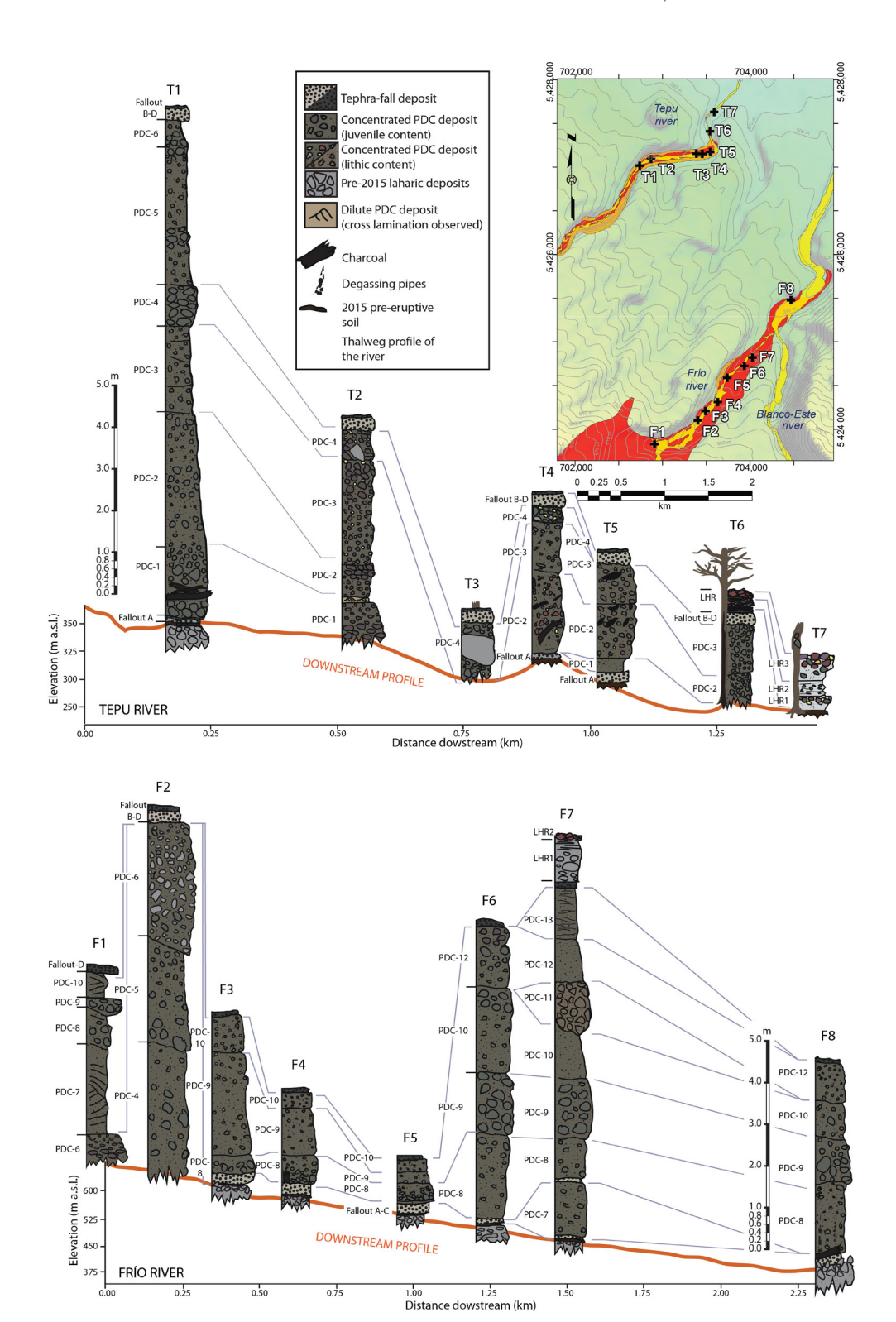


FIG. 2. Stratigraphy of PDC deposits in the Frío and Tepu valleys, including the location of stratigraphic sites. Correlation of profile descriptions in the Frío and Tepu study areas are presented.

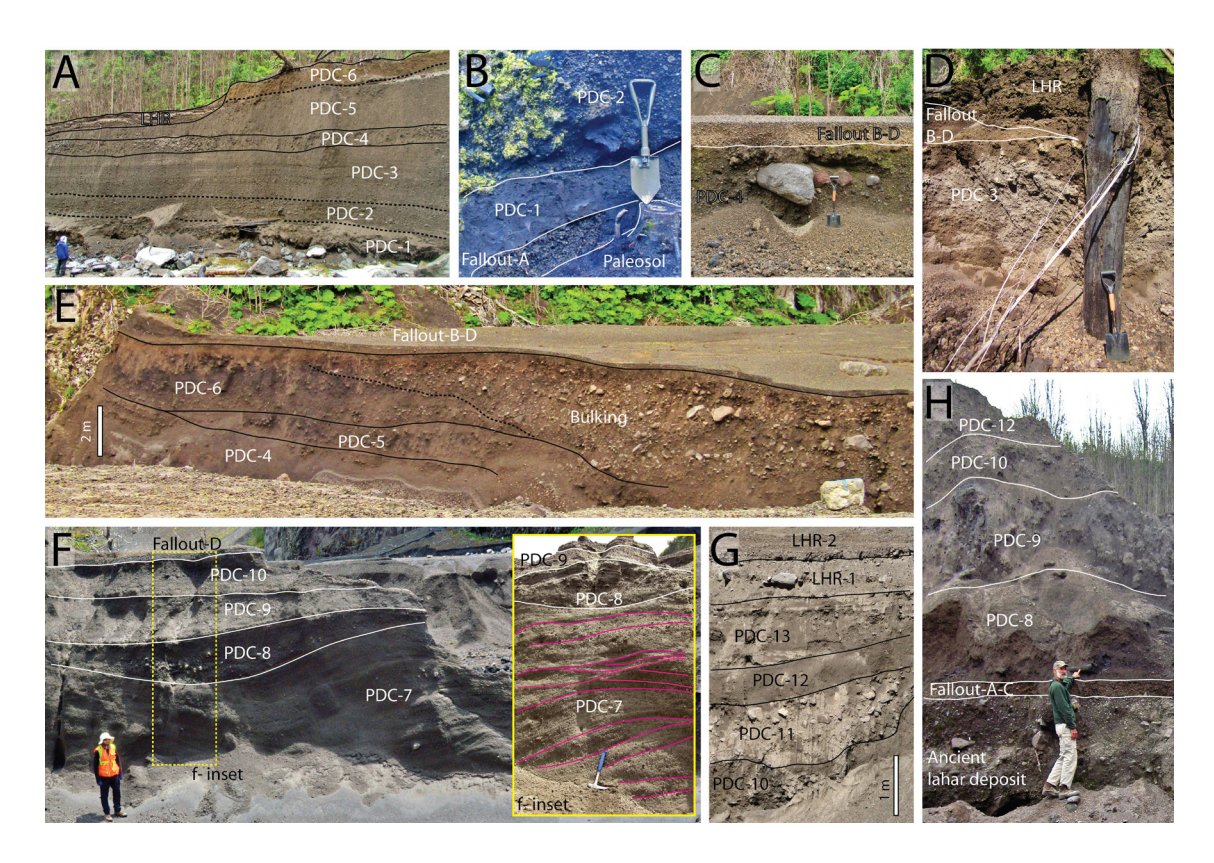


FIG. 3. Photographs of PDC and lahar deposits and associated tephra fall units in the Tepu (A-D) and Frío (E-H) valleys. A. Full sequence of pyroclastic units at section T1. B. Basal units overlying pre-eruptive soil at T5. C. Subrounded boulder-sized accidental lithics at T3. D. Standing tree buried by the PDC at T6. The upper part of the section corresponds to tephra fall and lahar deposits. E. Middle PDC section at the upper Frío river (F2) showing laterally discontinuous units, one of them exhibiting intensive bulking (PDC-6). F. Fine-grained and cross-stratified PDC beds intercalated by a coarser-grained PDC-8 unit at the upper Frío river (F1). G. Upper PDC section showing two lahar beds to the top (LHR1 and 2) at section F7. H. Composite stratigraphy of the uppermost PDCs at section F8 (Blanco river). Credits: J. Romero, with the exception of inset f (F. Sánchez, lines show cross stratification). PDC labels are correlated to these of figure 2.

this diameter criterion, we measured basal diameter (at ground level) and adjusted those measurements by a factor of -20% to estimate their DBH to account for taper, based on the relationship between basal diameter and DBH from 26 trees for which we had both measures. In four cases, we cut disks of wood at approximately 50 cm intervals along the lengths of tree boles to examine evidence of heat damage in relation to the depth of burial by PDC deposits. To interpret occurrence and consequences of dilute PDCs, we observed patterns of defoliated, upright, and toppled large shrubs and trees on hillsides above the top of the valley floor PDC deposits, noting size (diameter) and orientation of toppled trees/shrubs, charring, and sprouting of new foliage.

We also noted the thickness of associated PDC deposits, distribution of heat damage on trees and soil buried by PDC deposits, and fallen tree tops where they broke at the top of the PDC deposits. In order to assess how the thickness of PDC deposits affected toppling of upper portions of partially buried trees, we tallied 11 to 21 partially buried trees at each of the seven sites where deposit thicknesses ranged from 0.4 to 5.5 m. We selected sites where fluvial erosion had exposed the full thickness of the deposit and the remains of upright trees were still present within a few meters of the edge of the bank, so we could confidently estimate the deposit thickness pertained to all trees in the sample. For each tree, we noted the diameter at the top of the deposit, the

top fell, the direction of toppling, and evidence of burning or splintering at the break point.

# 2.4. Fumarole geochemistry and PDC emplacement temperature

To evaluate fumarole geochemistry, an active pipe in the front of the Blanco-Este PDC deposit was sampled on 11 May 2015, using a 1 m long titanium tube ( $\emptyset$ =2.5 cm) connected by quartz-glass dewar tubes to pre-evacuated 60 ml glass flasks equipped with a Teflon stopcock. The pre-evacuated and weighed flask was filled with 20 ml of a 4 N NaOH and 0.15 M Cd(OH), suspension to (1) condense water vapor and dissolve CO2, SO2, HCl and HF, (2) precipitate elemental sulfur and (3) combine H<sub>2</sub>S with Cd<sub>2</sub>+ to form insoluble CdS. The residual gases (N<sub>2</sub>, O<sub>2</sub>, CO, H<sub>2</sub>, He, Ar, Ne, CH<sub>4</sub>, and light hydrocarbons) were concentrated in the head-space. Subsequently, the temperature was measured directly in the fumarole, and in the stream discharged immediately in the front of the PDC deposit. The gas analysis was carried out in the Fluid Geochemistry Laboratory of the University of Florence, Italy, following the procedures of Vaselli et al. (2006). The eruption temperature was estimated by using H<sub>2</sub>/H<sub>2</sub>O and CO/CO, pairs as geothermometers.

In another assessment of emplacement temperature of deposits, eight representative samples of transported wood (charcoal) fragments that were entombed within PDC deposits in the Blanco-Este River valley downstream of the Frío River (site F8 in Fig. 1B) were analyzed to estimate charring temperatures. The use of charcoal reflectance data has proved to be an effective tool in determining the emplacement temperature of ancient PDC deposits (Scott and Glasspool, 2005; Scott et al., 2008; Hudspith et al., 2010; Pensa et al., 2018, 2019; Trolese et al., 2018). Samples ranged from 5 to 20 cm in diameter and were randomly collected at different stratigraphic positions and at different distances from the volcano summit.

Small crushed samples of charcoal were embedded in epoxy resin and wet-polished for viewing with reflected light microscopy. Polished sample preparation involved the use of grinding papers (grain size of 250, 500 and 1,000  $\mu m)$ , and alumina powders (grain size of 1, 0.3 and 0.01  $\mu m)$ . According to the standard procedure for coal petrography, samples were studied using a Zeiss Axioskop 40 microscope linked to a

MPS 200 detection system (J&M Analytik AG). Reflectance (Ro%) was measured under immersion oil of refractive index 1.518, using a tungsten-halogen lamp filtered to 546 nm and an Epiplan-Neofluar 50x lens. The instrument was calibrated by using different mineral standards, including spinel (Ro%=0.426), sapphire (Ro%=0.595), yttrium-aluminum-garnet (Ro%=0.905) and gadolinium-gallium-garnet (Ro%=1.726). The number of Ro% measurements on each sample varied from 30 to 120.

Similar analyses for samples from the Tepu River valley were carried out by Ricci *et al.* (2022) and these results are discussed with our observations.

#### 3. Results

# 3.1. Volcaniclastic stratigraphy

The 2015 eruption produced PDCs that flowed down many river valleys draining from the summit of the volcano (Figs. 1A and B). These PDCs inundated the Tepu valley, a 50-70 m wide sinuous fluvial channel, and the Blanco-Este Frío valley that was wide (150-300 m) and straight fluvioglacial valley, up to 50 m deep. These deposits cover an area of ~9.1 km², and our field observations reveal an average thickness of ~5 m. If extrapolated, this thickness gives an estimated volume of ~0.046 km³.

We studied PDC and lahar deposits at both Tepu and Frío valleys in fifteen sections, which are identified as T1 to T7 for the Tepu, and F1 to F8 for the Frío (Fig. 2). These individual units are composed of cauliflower-shaped bombs and lithics (Table 1), and are discriminated by their components, overall architecture and stratigraphic discontinuities (sharp or erosional contacts; Fig. 3). Only the uppermost PDCs found in the Frío valley could be correlated to the Tepu sequence (Fig. 2) using attributes of the deposits and their relation to tephra fall units, assuming that the A tephra fallout layer was deposited during the initial pulse and layers B to D were emplaced during the second pulse of the eruption (see Castruccio et al., 2016 for details). The maximum thickness of PDC deposits in the Tepu ranged up to 12-13 m, and the PDCs were composed of at least six flow units (Fig. 3A). It appears that the PDCs occurred during the onset of the eruption (first pulse) as tephra fallout unit A is overlain by these PDCs (Fig. 3B), which are covered by tephra units B to D (Sections T1 to T6 and F; Fig. 3C), being also observed at

TABLE 1. STRATIGRAPHY AND SEDIMENTOLOGY OF VOLCANIC AND VOLCANICLASTIC DEPOSITS ACCORDING TO THEIR RELATIVE CHRONOLOGY IN THE STUDY AREA.

Unit	Type	General description	Locality	
A	Tephra fallout	Reversely graded, medium-to-coarse gray lapilli fallout, with 74% low-density scoria, 23% high-density scoria, and 3% lithics. The largest juvenile particles are $2.4-2.7$ cm diameter and lithics reach $\sim 1$ cm.		
PDC-1	PDC	A 0.16 m-thick unit composed of fine to medium massive ash containing medium-sized lapilli clasts and abundant lithics (>50%) with reverse grading (Fig. 3B).		
PDC-2	PDC	Massive, matrix-supported unit of 1.3 m thickness (Fig. 3B), which contains cauliflower bombs of high density scoria (80%), low density scoria (15%) and lithics (5%).	T5	
PDC-3	PDC	1 m-thick unit composed of matrix-supported clasts of normally graded cauliflower bombs of high density scoria (70%), reversely graded low density scoria (20%) and ungraded lithics (10%).	T5	
PDC-4	PDC	0.4 m-thick of a clast-supported deposit containing cauliflower bombs of high density scoria (75%), low density scoria (15%) and few boulder-sized subrounded lithics (10%).	T1, T2, T3 and T4	
PDC-5	PDC	Thick (>2 m) unit composed of two sections characterized by reversely graded, matrix supported deposits containing cauliflower bombs and scarce lithics ( $<10\%$ ).	T1	
PDC-6	PDC	At Tepu River, it consists of varying amounts of boulder-sized, lithic fragments (generally up to 10-60% by volume), which were probably incorporated by bulking during passage of the PDCs down the valley (Fig. 3C, D). At the Frío River, this unit displays a lateral transformation containing angular, block-sized, accidental lithics which account >60% of the fragments (Fig. 3E).	T1 and F1	
В	Tephra fallout	Ungraded, coarse lapilli fallout with a few bombs, containing $\sim\!60\%$ low-density scoria, 37% high-density scoria and 3% lithics. The largest juvenile particles are 3.4-3.7 cm and lithics reach $\sim\!1$ cm.	Most of sections	
PDC-7	PDC	Dune-bedded, cross-stratified and matrix-supported non-welded pyroclastic units (Fig. 3F) containing 50% low-density scoria, 46% high-density scoria and 4% lithic fragments, all of them of fine-to-medium lapilli size.	F1	
C	Tephra fallout	Reversely graded, medium brown lapilli fallout, with $\sim\!61\%$ low-density scoria, 37% high-density scoria and 2% lithics. The largest juvenile particles are 1.8-2.3 cm diameter and lithics reach 1.1 cm.	Most of sections	
PDC-8	PDC	Contains reversely graded cauliflower bombs and lithic blocks supported by a fine-to-medium ash matrix with degassing pipes and carbonized material (Fig. 3H).	F6, F7 and F8	
PDC-9	PDC	Massive, coarse-grained unit containing abundant cauliflower bombs up to $60~\rm cm$ in diameter, and few metric-sized lithics (Fig. 3G and H).	F1, F6, F7 and F8	
PDC-10	PDC	Massive, reversely graded, coarse-grained unit containing cauliflower bombs and scarce lithic fragments.	F6, F7 and F8	
PDC-11	PDC	Consists of a massive, fine-depleted, clast-supported channelized lithic breccia unit, containing sub-angular metric blocks (Fig. 3G).	F7	
PDC-12	PDC	Unit composed of a lowermost section containing lithic-rich, fine lapilli fragments, grading upwards to a massive, coarse-grained deposit with metric cauliflower bombs and lithic fragments within a fine-to-medium ash matrix (Fig. 3G, H).	F6, F7 and F8	
PDC-13	PDC	Consists of a fine-to-medium ash matrix supporting lapilli-sized fragments and lithics up to block size with reverse grading (Fig. 3G). The upper half shows lamination.	F7	
D	Tephra fallout	Ungraded, medium lapilli fallout, containing $\sim$ 71% high-density scoria, 25% low-density scoria and 4% lithics, with 3% of hydrothermally altered lithics. The largest juvenile particles are 1.9-2.2 cm diameter and lithics reach 1.2 cm.	Most of sections	
LHR1	Lahar	Clast-supported, coarse grained and reversely-graded diamict with oligomictic to polymictic components, generally eroding unit D (Fig. 3D, G, and Supplementary Fig. 1).		
LHR2	Lahar	Matrix supported, well stratified diamict containing oligomictic to polymictic clasts medium-to-coarse sized with reverse grading (Supplementary Fig. 1A, B).	T7 and F7	
LHR3	Lahar	Coarse grained, matrix-to-clast supported massive diamict with metric sized angular polymictic boulders.	River bed at T1 and F6.	

Scoria is described accordingly to Arzilli et al. (2019).

the uppermost Frío PDCs (Fig. 3E). The Frío PDCs consist of four to seven flow units with maximum deposit thickness of 10 m, but the middle and lower sections overlie the tephra fallout layers A-C, and they have layer D on top (F3 to F8; Fig. 3F, H), thus suggesting their emplacement during the second pulse of the eruption.

The Tepu PDCs (T1 to T7; Fig. 2) consist of up to six massive flow units (Fig. 3A) that directly overlie the vent-opening tephra fallout (A; Fig. 3B) and contain unsorted, matrix-supported, sub-rounded to cauliflower-shaped dense scoria bombs of black, brown or reddish scoria up to 70 cm diameter and minor denser blocks of non-juvenile rocks (i.e., accidental lithics; Fig. 3C), which were probably ingested from the former river channel. Despite at stratigraphic column T5 (Fig. 2) not all the PDC units are observed, the good preservation of the pre-eruptive ground and the initial tephra fall deposit allows a careful description of the lowermost stratigraphy of the sequence (e.g., Table 1). The basal PDC unit (0.16 m thickness) is composed of fine to medium massive ash containing lapilli clasts with reverse grading (Fig. 3B). This is overlain by a massive, matrix supported PDC unit of about 1.3 m thickness (Fig. 3B), which contains clasts of high density scoria (80%), low density scoria (15%) and lithics (5%). Above, another PDC unit of 1 m thickness consists of matrix-supported clasts of normally graded high density scoria (70%), reverse graded low density scoria (20%) and lithics (10%), covered by at least 0.4 m of a clast-supported PDC deposit containing high density scoria (75%), low density scoria (15%) and lithics (10%). Two units are enriched in boulder-sized lithic fragments: PDC-4 and PDC-6. However, the lithics are dominantly subangular in PDC-6 and up to 10-60% by volume, which were probably incorporated by bulking during passage of the PDCs down the valley (Fig. 3C, D). The PDC deposits are covered by tephra fallout deposits (layers B to D; Fig. 3C), which were subsequently eroded by lahar deposits (Fig. 3D). The largest accidental lithic blocks occur toward the top of the PDCs at the upper Frío valley (Fig. 3E), however they are laterally discontinuous. The occurrence of multiple PDCs in the Tepu is indicated by discontinuities in the deposit stratigraphy. Contacts with the coarser-textured, massive PDC deposits are sharp and erosional in some cases (Fig. 3E).

After the eruption, both Tepu and Frío were affected by lahars, forming thin (<1 m-thick) matrix- to

clast-supported and reversely-graded oligomictic to polymictic diamicts; these lahars flowed downvalley on top of the fall unit D, or through newly formed incisions within the 2015 PDC deposits (Fig. 4). At least three laharic deposits have been identified in these two valleys, and they contrast between granular flows (LHR1 and LHR3) and hyperconcentrated flows (LHR2), as interpreted from their internal sedimentary structures (Table 1).

#### 3.2. Fumarole extension and deposit erosion

Fumarole activity, an indication of presence of water and deposit cooling, varied over time after the eruption. Fumaroles were weak, but present even as early as 23 April in both the Frío and Tepu valleys as observed in the Google Earth images, but rapidly increased between 27 April and 4 May (Fig. 5A to D). Initially, the Frío valley floor was flat-topped, covered with primary PDC and tephra fall deposits, fumaroles were very limited, and streamflow occurred only along the eastern margin of the valley (Fig. 5E). During field visits to the Frío valley on 6 May and 4 June 2015, abundant fumarole activity was observed across the surface of the PDC deposits in the form of steam plumes and pools of hot mud, forming 1-2 m diameter patches of precipitate around degassing pipes (Fig. 5F). By 11 May, the outlet temperature of the fumarolic discharges was 241 °C. Gas composition was characterized by predominance of water vapor (98.7 mol %) and the dry gas concentration reached up to 1.3 mol %. Dry gases were dominated by CO<sub>2</sub> (907,030 µmol/mol), H<sub>2</sub> (65,000 µmol/mol),  $N_2$  (16,000 µmol/mol), hydrogen sulfide (8,600 µmol/ mol) and methane (2,400 μmol/mol), whereas acid species, such as SO<sub>2</sub>, HCl and HF, were absent. Those species have a very high solubility (Giggenbach, 1996), and, considering the interaction of the PDC with the stream, a complete solubilization on contact with water is expected. Fumarole activity was very rare and feeble when we visited the Frío and Tepu sites on 28 Jan 2016, 8 months after the eruption (Fig. 5G), however light-gray patches of precipitates on the PDC deposit surfaces were widespread (Fig. 5H).

The precipitation record (Fig. 6) gives an indication of the probable amount and timing of water available to erode the new deposits and support fumaroles. The eruption occurred at the transition from the dry to the wet season, and  $\sim 300$  mm of rain fell in the four weeks before the eruption.

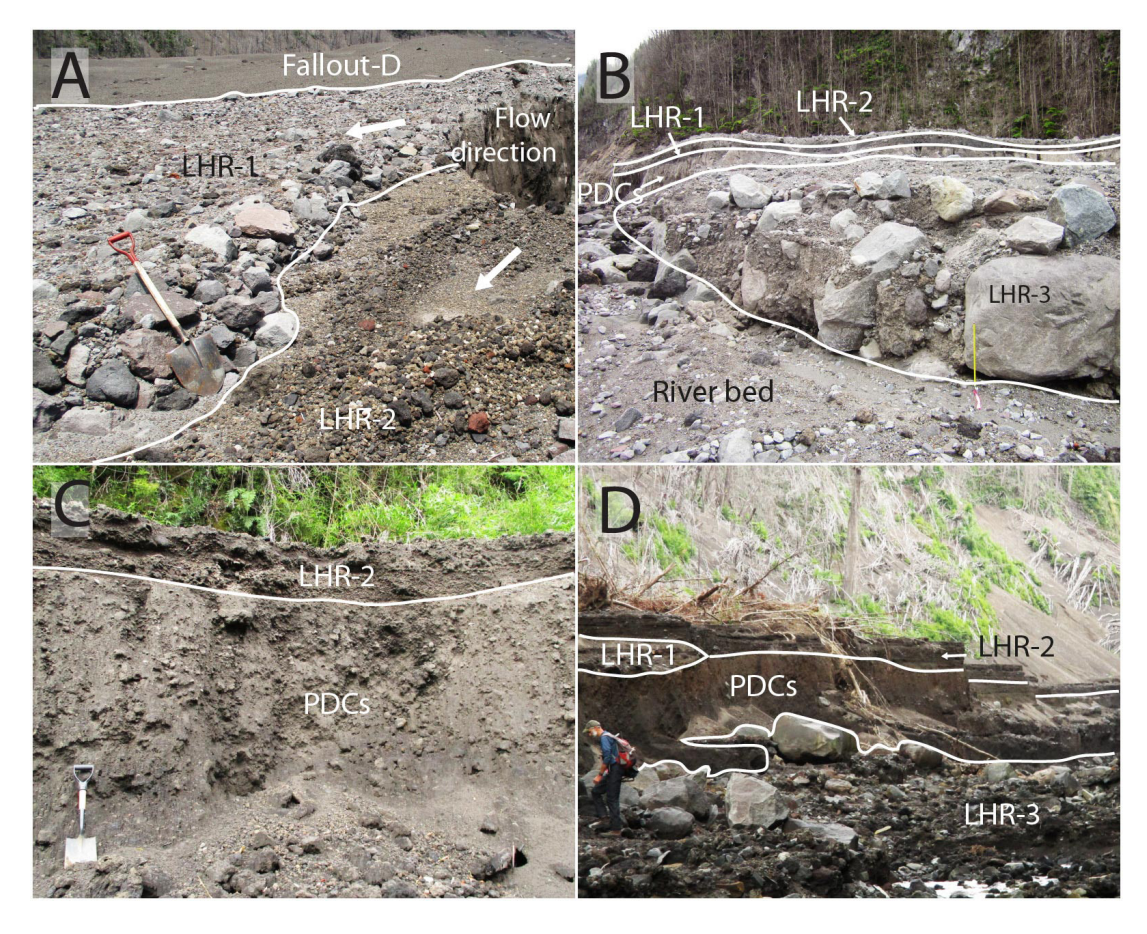


FIG. 4. 2015 lahar deposits in both Frío (A-B) and Tepu (C-D) rivers, lying on top of PDCs and in gullies generated by the erosion into these PDC units.

Significant precipitation events did not begin for several weeks after the eruption, when a sequence of four precipitation events >20 mm occurred between 15 May and 15 June. Using the relationship between the elevation and the rainfall calculated for the study area, we estimate that in the rainiest 10-day period ~50 mm fell at the Frío study site (mean elevation 500 m a.s.l.) and >80 mm fell at the Tepu study area (mean elevation 315 m a.s.l.). By 5 May, the volcano was already covered in snow above 1,600 m a.s.l.

Photographic records of the Frío River document that significant fluvial erosion occurred between 6 May and 4 June (Fig. 5E), coincident with the larger precipitation events (Fig. 6), and erosion continued during 2016 and 2017 (Fig. 7A). By January 2018, the Frío River channel bed comprised large, subrounded boulders of a variety of rock types, which, along with the presence of an exposed water-supply

pipe (Fig. 7B), suggested that erosion had reached the pre-eruption streambed. Evidence of the preeruption stream banks in the form of remnants of soil and root systems was extremely rare.

Fluvial erosion of the lower Tepu PDC deposits had proceeded to a depth of several meters by 27 May, but had not reached the pre-eruption channel or valley floor surface. By January 2016 channel incision in the lower Tepu had proceeded to the pre-eruption streambed and stream banks in some areas (Fig. 7C), but by January 2019, extensive lateral and deep downward erosion of PDC deposits was observed exposing more of the channel in its pre-eruption position (Fig. 7B). The pre-eruption channel was identified by (a) the large, sub-rounded boulders of various rock types in the exhumed streambed and banks, (b) the roots of killed streamside trees marking the location of the stream banks, and (c) the remains

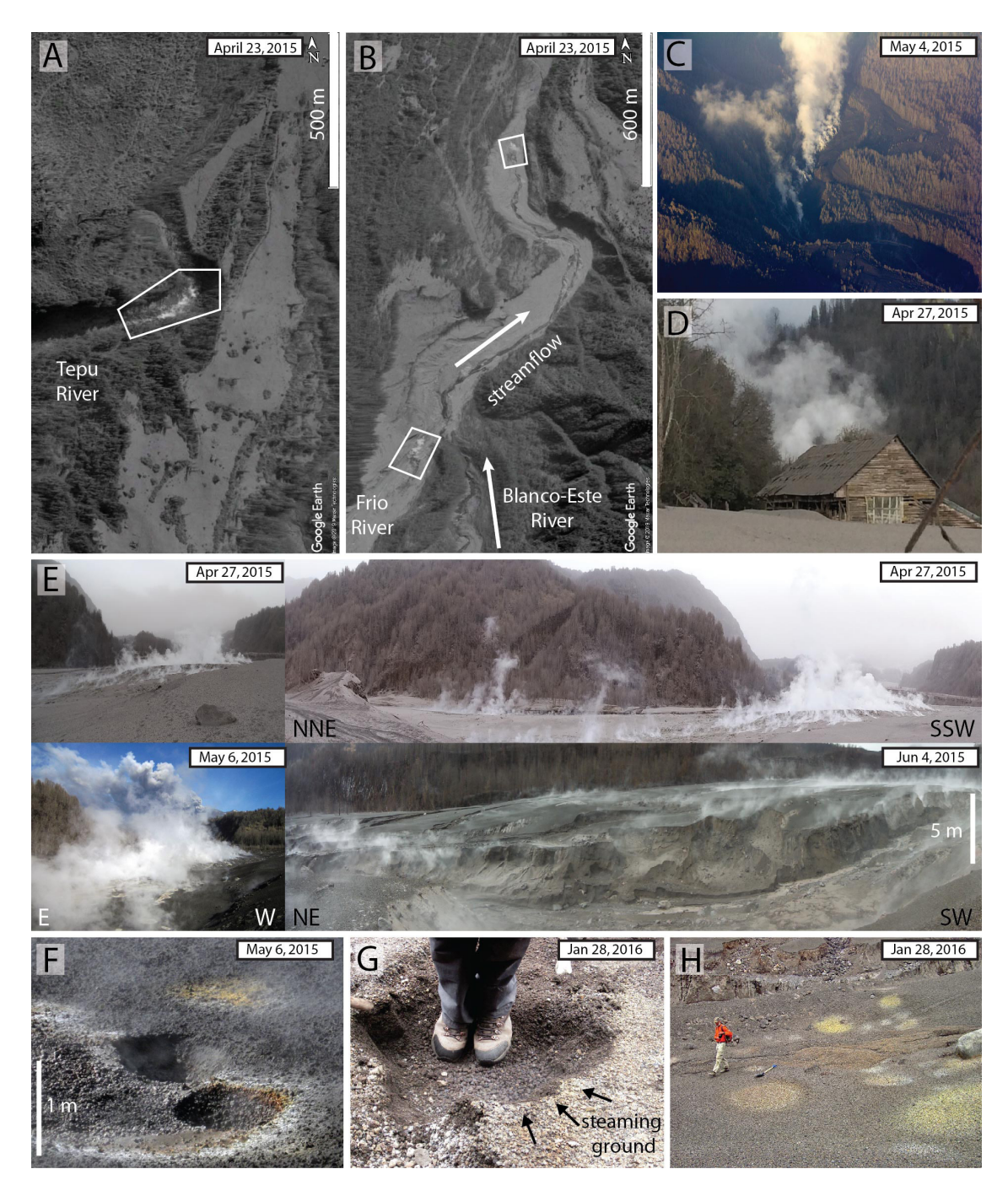


FIG. 5. Fumarole activity and progress of fluvial erosion of the 2015 PDC and lahar deposits in the Frío and Tepu river valleys. Google Earth™ satellite images of both rivers on 23 April 2015 are shown in **A** and **B**. **C**. Aerial view of PDC deposits and their associated fumaroles in the Frío river (Diego Spatafore). **D**. Fumaroles in the Tepu valley by 27 April 2015 (Bárbara Corrales). **E**. Fumarole activity and fluvial erosion in the Frío valley during April-June 2015 (D. Morgavi and C. Valenzuela). **F**. Detail of degassing pipes in the surface of the PDC deposit in the Frío valley. The diameter is about 1 m. **G**. Steaming ground in reworked tephra fall deposits covering PDC deposits of the upper Frío valley. **H**. Fumarolic patches in the upper Frío River.

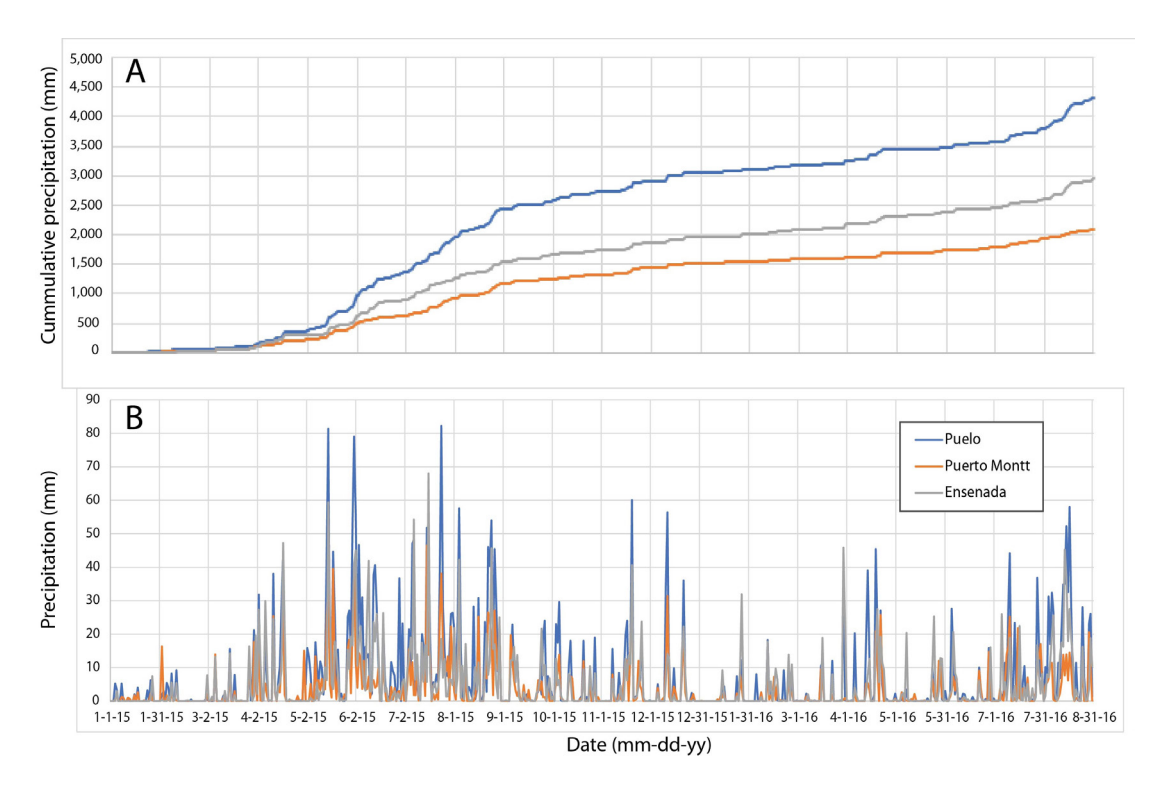


FIG. 6. Records of cumulative **A** and daily **B** precipitation at three gauging stations: Ensenada 10 km northeast of Calbuco (41°13'39.60" S; 72°34'4.53" W, 62 m a.s.l.), Puerto Montt 32 km southwest of Calbuco (671,522 E, 5,407,833 N, 90 m a.s.l.) and Puelo 45 km southeast of Calbuco (41°27'45.97" S; 72°56'46.17" W, 5 m a.s.l.). Mean annual rainfall at these stations is 2,473, 2,046 and 2,956 mm, respectively. Source: Servicio Hidrométrico Nacional. https://dga.mop.gob.cl/Paginas/hidrolineasatel.aspx.

of the pre-eruption forest floor and shallow rooting zone on the exposed floodplain surface adjacent to the stream bank. Sediment released by erosion of the new PDC, lahar, and tephra fall deposits in both Frío and Tepu was delivered to the Blanco-Este River (Fig. 7D), and the outlet of Tepu, the latter forming a 3-m thick delta into Llanquihue Lake (Fig. 7E).

## 3.3. Conditions of forests affected by PDCs

The trees and shrubs in the upper Frío River at the time of the eruption appear to have been smaller and less dense than in the Tepu. In Google Earth imagery of 9 March 2012 and 10 January 2014 the Frío valley floor appears to have had a deeply incised channel with shrubby vegetation bordered by a broad terrace with very limited vegetation. Tall shrubs and small trees were more abundant on the Tepu valley floor, as evident in the same Google Earth imagery, by our observations of remnants of vegetation exposed by fluvial erosion, and confirmed

by local residents. For example, in the three plots A-C of remnant vegetation in the Tepu valley the number of stems ranged from 51 to 83 in the 300 m² plots and only 5 out of the 199 stems exceeded 16 cm DBH (Table 2). Mean DBH was 6 to 8 cm, and basal area ranged from 0.26 to 0.46 m²/300 m². Plot D, located downstream of the PDC deposits and fluvial disturbance, had substantially higher stem density and mean basal area, but the mean DBH and the frequency of trees with DBH >16 cm are similar to the plots in the PDC-affected zone.

In the Frío River valley, partially buried, dead trees occurred only along the margins of the deposits in the study reach (within 30 m of the valley wall) (e.g., Fig. 8A). In the Tepu valley, the larger (DBH >16 cm), partially buried trees remained standing at some locations along the margins of the valley floor (Fig. 8B) and also at the distal end of the PDC deposits (lower 500 m), where upright, emergent boles of trees were buried by up to 4 m of PDC deposits (Fig. 8C). All trees that were partially



FIG. 7. Evolution of the fluvial incision in the Frío (A) and Tepu (B-C) river valleys and sediment delivery at the Blanco-Este River and Llanquihue Lake (D-E) some years after the eruption. (Photos a to d by J. Romero and photo e by C. LeRoy).

buried by PDC deposits, even only a few 10s of cm of deposits, were killed in both study sites.

We searched for evidence that the PDC had sufficient impact force to uproot and transport trees down the valley. In the Tepu valley sample plots where PDC deposits had been removed by fluvial erosion, we observed many tipped trees (Fig. 8C), but no cases of pits in the pre-eruption soil where root systems may have been pulled out. In a few cases, we observed large (up to 30-cm diameter and 5+ m long), thoroughly-charred tree stems incorporated within PDC deposits, but they lacked attached root systems. We also did not observe deposits of transported large pieces of wood at the front of the PDC deposits. Collectively, these observations constitute a lack of evidence that the PDCs uprooted trees and push them down the valley to a significant extent.

Some of the upper parts of partially buried trees broke off at the top of the PDC deposits, and in some

cases charring of splintered ends had occurred over 20-30 cm of the length of the tree stem in the zone of breakage (Fig. 8D). However, others toppled tree tops lacked evidence of charring. In most, but not all cases, the tops fell in the down-valley direction. In the Tepu valley, the fallen tree tops are located on either the fluvially-eroded surface or on top of the PDC deposits capped with ~30 cm of tephra fall deposits (Fig. 8C, D). The fallen tree tops retain their branch systems, which are not charred (Fig. 8D). In some cases, pieces of scoria up to 40 cm in diameter are perched among the branches, and the bark is removed from upstream-facing surfaces of limbs (Supplementary Fig. 1). We have observed no evidence of sprouting of trees with PDC deposits at their base, but herbs, shrubs, lichens, and moss have colonized to varying extent on the surfaces affected by volcanic and fluvial processes years after the eruption (Fig. 8E).

TABLE 2. PROPERTIES OF WOODY VEGETATION (BASAL DIAMETER >5 CM) IN THREE PLOTS (A-C) (50-M LONG AND 6-M WIDE ORIENTED PARALLEL TO THE VALLEY AXIS) IN THE ZONE OF PDC DEPOSITS IN THE TEPU AND ONE PLOT (D) LOCATED 1 KM DOWNSTREAM OF THE PDC DEPOSIT ZONE IN AN AREA UNAFFECTED BY PDCS OR FLUVIAL DISTURBANCE IN 2015.

Property	Plot A	Plot B	Plot C	Plot D
total stems	83	51	65	139
basal area (m²/300 m²)	0.26	0.40	0.46	1.23
DBH (cm)				
max	12	46	36	33
min	4	4	4	4
mean	6	8	8	10
stdev	2	6	5	4
height of tip (cm)				
max	110	180	160	n/a
mean	24	71	54	n/a
min	0	18	0	n/a
length of stem (cm)				
max	210	600	200	n/a
mean	69	226	72	n/a
min	7	70	9	n/a
DBH if upright (cm)				
max	-	-	36	33
mean	-	-	18	10
min	-	-	10	4

All stem diameters are reported as DBH (diameter at breast height, 137 cm), based on conversion described in the text. No data are shown for DBH of upright stems at Plots A and B because no upright stem extending above the top of the PDC deposits existed. No data are shown for height and length of tipped and truncated stems in Plot D, because no stems of those types existed there.

Along study sections of the Tepu, localized patches of defoliated shrubs and trees were standing or fallen in a down-valley direction at locations up to 50 m above the top of the PDC deposits on the valley floor (Fig. 8F). These patches were most evident in the first several hundred meters downstream of the 20-m high waterfall in Tepu, and they were highest on the outside of bends in the orientation of the valley (Fig. 8G). Some trees and shrubs in these patches were sprouting a few years after the eruption. Discontinuous lenses of fine-textured, matrix-supported, crosslaminated and lapilli-bearing tephra layers (Fig. 8H) were found at various locations at the top, within, and below the concentrated PDC deposits on the valley floor. These observations appear consistent with deposition by dilute PDCs.

## 3.4. Charring patterns in trees

The tendency of the upper portions of the tree to have fallen varied with PDC deposit thickness and tree diameter. Trees that remained standing above the PDC deposits surface were relatively large (mean DBH 18 cm, Fig. 9A). At the site with 0.4 m of deposit (Fig. 9A), all trees remained standing with upright tops. At sites with 4.5 and 5.5 m of PDC deposits, all trees had fallen tops and most had evidence of burning at the breaking point at the top of the deposit. At sites of intermediate deposit thickness (2 to 3.5 m), tree responses were mixed, but smaller diameter trees were more likely to have fallen tops and evidence of burning in the zone of breakage. Smaller trees were tipped down-valley

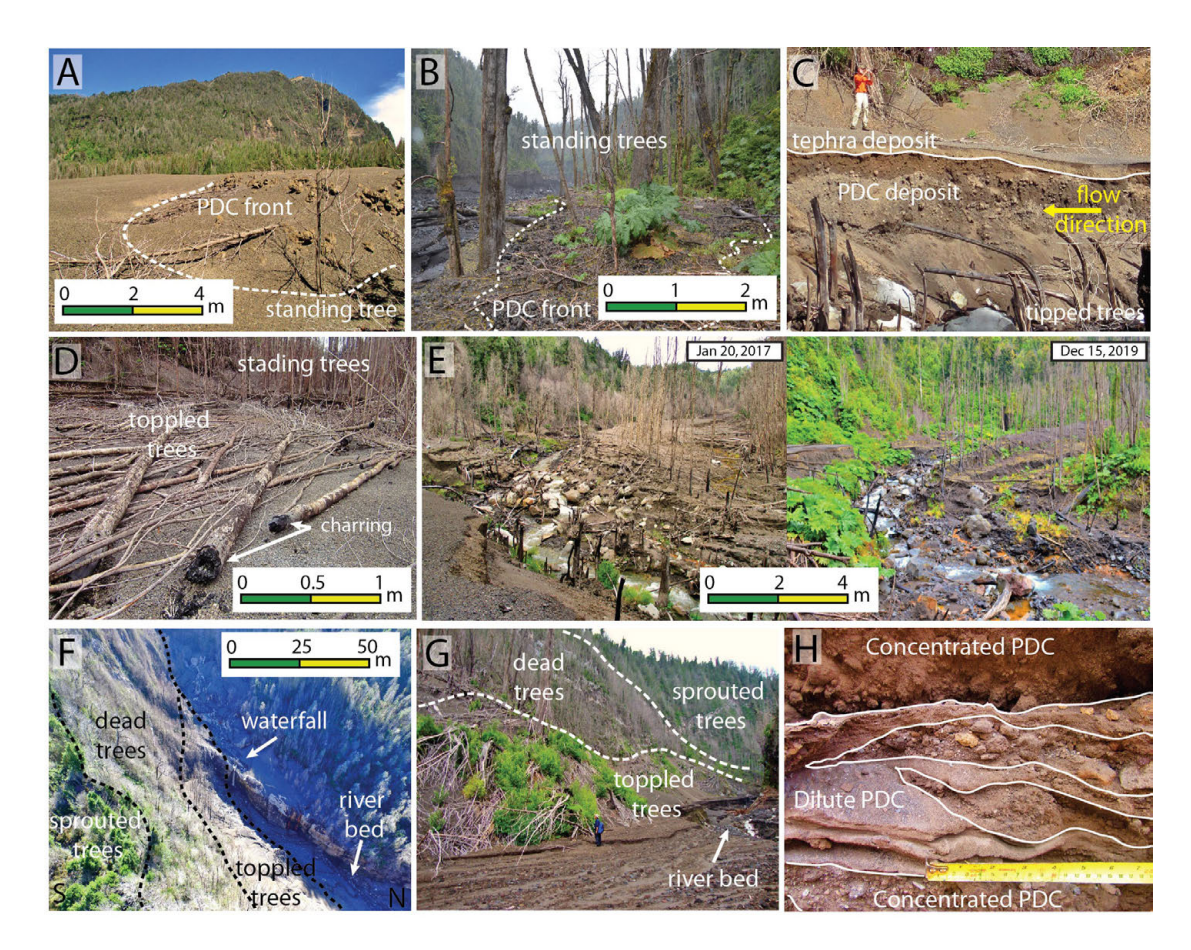


FIG. 8. Vegetation affected by PDCs. A. Dead trees along the margin of the Frio river, in the front of a PDC deposit; down-valley direction is toward the viewer (Nov 2016). B. Standing dead trees to the west side of Tepu valley, partially buried in the front of a PDC deposit (Dec 2019). C. Tepu Plot B area, small stems tipped down-valley and truncated ~1 m above the former ground surface (located at the feet of the person). The PDC deposit was eroded and stems are exposed next to the current river bed. D. Toppled trees above the surface of the PDC deposit in Plot B area at Tepu River. Most of the tree tops fell down the valley direction and charcoal is observed at their bases. E. New vegetation in the lower Tepu valley between 2017 and 2019. View looking upstream. F. Aerial view of toppled, dead and sprouting trees near a waterfall in the Tepu River (Pablo Saummann). G. Hillside with vegetation toppled by dilute PDCs in the upper part of the Tepu study section. View is looking upstream. Note sprouting on toppled trees during Jan. 2017. H. Dilute PDC between two concentrated PDC units at the Tepu site showing their internal architecture (white lines), including cross stratification and lenses of coarser particles.

at their base (Fig. 8C), and the tips were charred, frequently bent, and broken off, commonly at a diameter of 4-6 cm. The tips of these bent and broken stems were close to the pre-eruption ground surface (24 to 71 cm), and the mean length of these stems was up to three times greater than the mean height of the tips.

A 15-cm DBH sectioned tree near location T5 that remained standing, despite partial burial with 2.4 m of PDC and tephra fall deposits, displays increasing charring and radial fracturing upward from the

pre-eruption ground surface to the top of the deposits (Fig. 9B). At the top of the deposit, the top of the tree broke off and fell onto the primary deposits. The base of the broken tree top is charred, but a section of the tree top 20 cm above the break point shows very limited charring, and sections at 50 and 100 cm above the break point do not appear charred or discolored (Fig. 9B). In contrast, wood fragments (commonly <10 cm in diameter and <40 cm long) that were transported and contained in the PDC deposits are fully converted to charcoal (Fig. 9C).

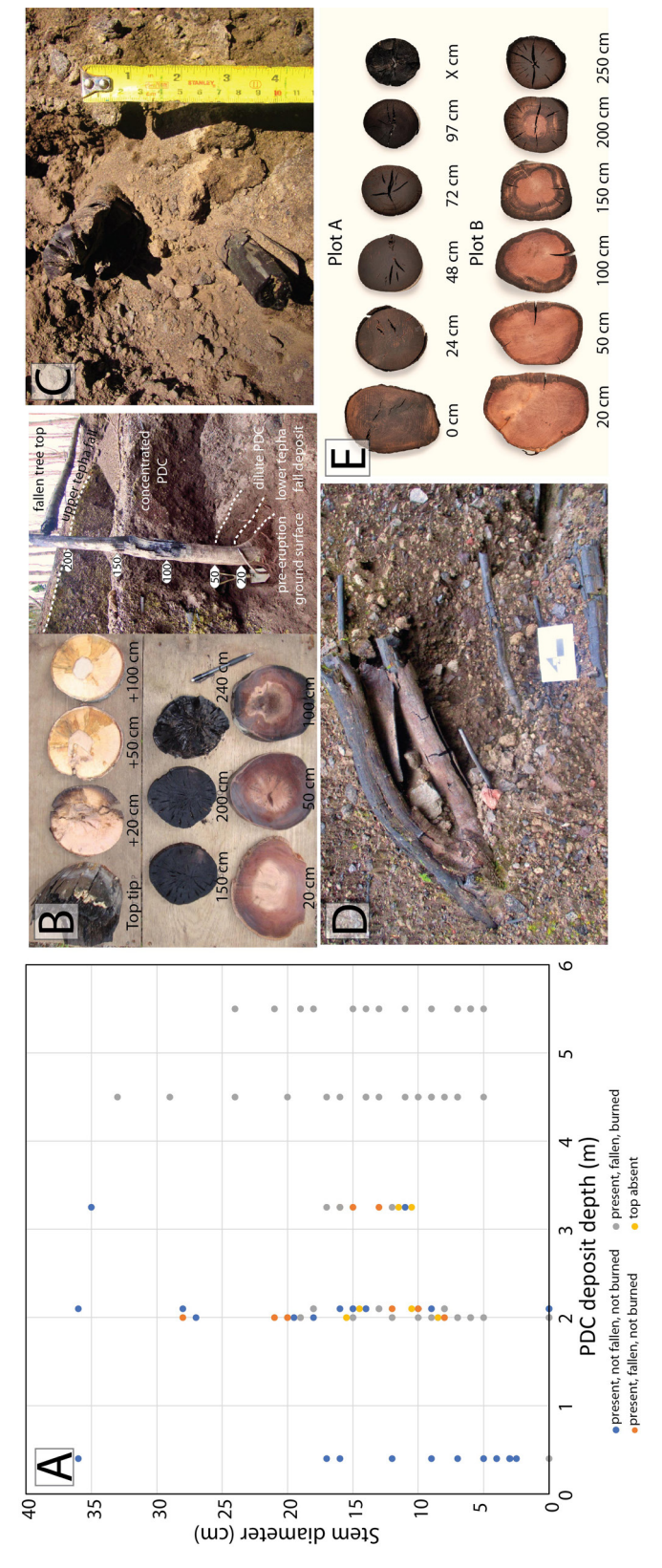


FIG. 9. A. Effects of stem diameter and PDC deposit thickness on the likelihood of an emergent tree top to fall or remain standing and for the point of breakage to be charred. Absence of a top is noted in cases where it may have been floated away by the river. Stem diameter is measured at the top of the PDC-tephra fall deposit. B. Cross-sections cut from a standing tree shown in photograph to the right located at site T5. The tree is buried in 2 m of PDC deposits capped with 40 cm of tephra, and the top has fallen to the right, resting on the uneroded deposits. Sections were cut at: (left, lower row) 20, 50, 100 cm above pre-eruption ground level; (middle row) 150, 200 cm above ground level and the burnt and broken top of the tree; (upper row) lower end of the broken upper part of the tree, and sections cut 20, 50, 100 cm above the broken tip of the upper, fallen part of the tree. Sections 50 and 100 cm up D. Bent over small, rooted trees at site T4. E. Cross-sections cut from two small trees tipped down-stream and truncated at their tips (right-hand section). Disks in the upper sequence are from a tipped over, 97-cm-long stem in Plot A, and numbers note position along the stem above the pre-eruption ground surface. The far right piece is the broken tip. Disks in the the stem from the break point show signs of decomposition at the sample date 32 months after the eruption. Shovel is 44 cm long. C. Charcoal fragments in PDC deposits at site T6. lower sequence are from a 240-cm-long stem located 100 m down-stream of Plot B and numbers note position along the stem above pre-eruption ground surface. Credits: F. Swanson. D.P. Bayles and J. Romero.

Rooted tree stems buried in PDC deposits exhibit heat effects, which vary with height above the preeruption ground surface. This is evident in cross sections cut from two small, tipped over, rooted trees that did not extend above the 4 to 5-m thick PDC deposits that buried them (Fig. 9D). Sections from close to the ground had minor discoloration and a pungent odor, while those from further above the ground surface were significantly charred (Fig. 9D). Completely charred transported wood fragments occur adjacent to the sectioned, upright tree, where crosssections display little or no charring in their wood at the same height above the pre-eruption ground surface. Charring patterns on the exterior surfaces of trees also exhibit increasing char up the stem within the deposit. Relatively large, standing trees in Plot C, for example, have greater char on the upper two thirds of the buried part of the stems than in their lower third (Fig. 9B). Charring was generally superficial blackening and not severe enough to remove wood.

Evidence of heating of soils below PDC deposits is extremely limited. Charring and discoloration of organic matter extends to a maximum of only a few cm into the pre-eruption floodplain soil at Plots A-C. At the site of the sectioned site (T5; Fig. 9B, E), a 16-cm-thick tephra unit rests on the pre-eruption soil surface and beneath the PDC deposits. Foliage of *Eucryphia cordifolia* and *Nothofagus dombeyii* within the tephra unit are not charred, nor is the underlying pre-eruption soil.

Abrasion of bark affected the up-valley side of some of the standing trees in some areas of the Tepu valley. Both passage of PDCs and bed load transport during fluvial erosion may have caused the abrasion. In some cases these processes could be distinguished; for example, where a tree in a zone of fluvial erosion was abraded, but a nearby tree still partially buried in PDC deposits was not.

# 3.5. Eruption and emplacement temperature determinations

According to the gas geothermometry based on the  $\rm H_2/H_2O$  and  $\rm CO/CO_2$  pairs geothermometers (Supplementary Table 1), we calculated a temperature range between 540 and 603 °C, assuming that equilibrium was attained under magmatic conditions controlled by the  $\rm SO_2/H_2S$  gas buffer.

All samples from the vicinity of the Frío study area (point F8, Fig. 1B) display measurable

Ro% values, indicating that they were exposed to temperatures greater than 200 °C (Scott and Jones, 1991), as below this temperature the Ro% cannot be measured. However, accurate taxonomic identification of charred specimens was not attempted for this study, but the large vessels in the cellular structure suggest the presence of several angiosperm species (Fig. 10A, B; Hudspith et al., 2010). Results from the reflected light microscopy analysis revealed the occurrence of fully charred materials, with a mean Ro% that ranges from  $1.51\pm0.07$  to  $2.88\pm0.08$ (Fig. 10C, D). Despite this relatively great extent in Ro% values, the Ro% distribution within each sample was distinctively unimodal with a low standard deviation (Fig. 10C, D), suggesting that the charring process persisted long enough to reach a stable point and equilibrate with the deposit temperature in that specific location. According to the experimental studies concerning the formation of charcoal (e.g., Ascough et al., 2010; Scott and Glasspool, 2005, 2007), our Ro% data translate into emplacement temperatures that vary from ~400 to ~550 °C.

#### 4. Discussion and conclusions

#### 4.1. Mechanism and dynamics of PDCs

The estimated volume of PDCs lies among the previous approximations (0.01-0.07 km³ in Mella et al., 2015; Castruccio et al., 2016; Van Eaton et al., 2016). Two mechanisms could explain the different pyroclastic units observed within the PDC sequence: the first corresponds to partial column collapse, which transported tephra down steep, headwater valleys, forming PDC units 1, 7, and 13. A second mechanism may include the syn-eruptive remobilization of proximal fall deposits, emplaced primarily as ballistic bombs (e.g., Risica et al., 2022) that formed bomb-rich units (e.g., PDC units 2-10, and 12). The Tepu PDCs are bracketed by the B, C and D tephra fall deposits, so they were emplaced within a period of 1.5 hours, during the first eruption pulse (Castruccio et al., 2016), while at Frío these flows seem to have occurred during both the first and second pulses. Taking into account a pre-eruptive magma storage temperature of 900-950 °C (Arzilli et al., 2019; Morgado et al., 2019), and the fast kinetics of H<sub>2</sub> and CO (Giggenbach, 1987), the range of temperatures calculated here would represent the original temperatures of these PDCs.

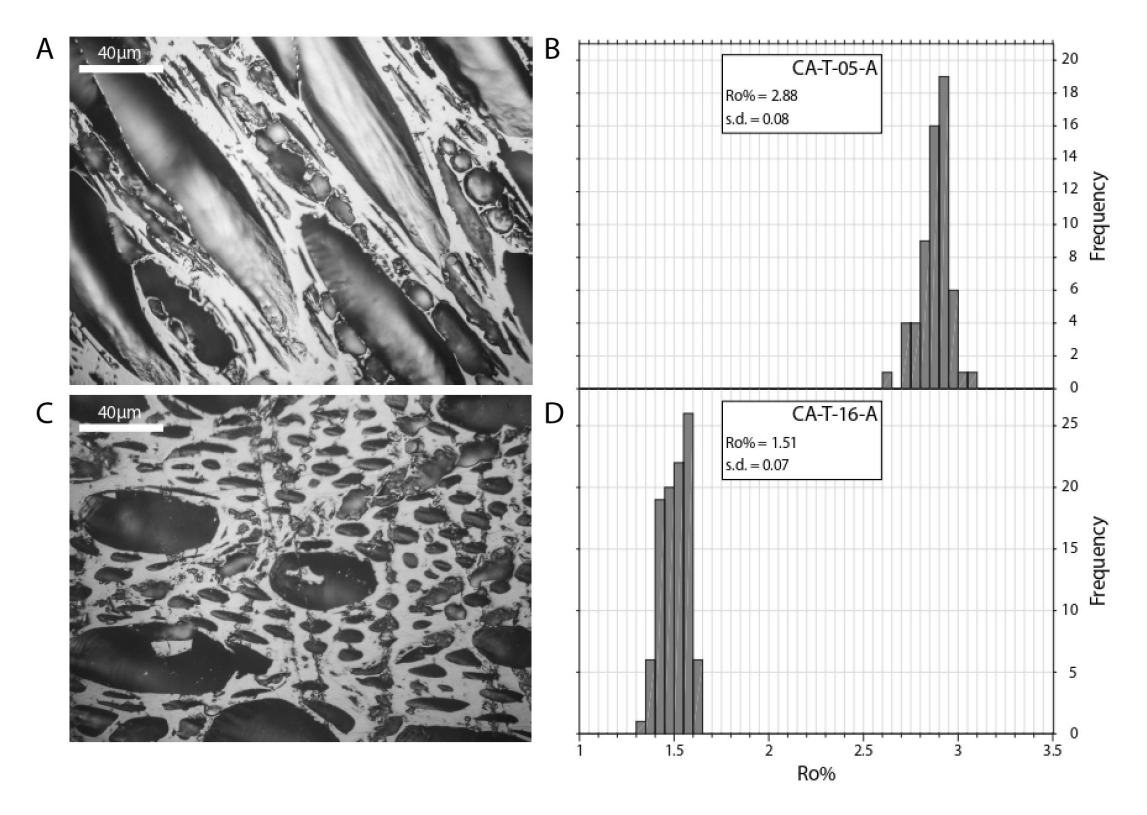


FIG. 10. Reflectance photomicrographs of polished blocks under oil of charcoal samples CA-T-05-A (**A**) and CA-T-16-A (**B**), showing the presence of large vessels in the anatomical structure. Frequency histograms (expressed in %) showing the distribution of Ro% values for samples CA-T-05-A (**C**) and CA-T-16-A (**D**) Mean Ro% values and relative standard deviations are shown in the inset of each sample.

The ground-hugging phase of these PDCs displays sedimentologic characteristics in agreement with concentrated flows (e.g., moderate grain fabrics; Branney and Kookelar, 2002). In some cases, large (i.e., up to 1.5 m) lithic blocks are incorporated at Tepu, but they are more common in the Frío PDCs, forming lithic breccias indicative of intense flow bulking or abrupt changes in the eruptive style due to lava dome collapse, plug failure, conduit erosion, or the opening of new vents (e.g., Cioni et al., 2004; Caricchi et al., 2014; Major et al., 2013; Furukawa et al., 2014; Romero et al., 2017; Yasuda and Suzuki-Kamata, 2018). The identification of multiple units leading to a stepwise aggradation of the deposits (see Sulpizio et al., 2014) can be interpreted as the occurrence of a succession of PDC pulses, also producing lobate fronts in terminal deposits due to pulse stoppage. This is in agreement with the model of small-scale PDCs of Sulpizio (2007). These granular, concentrated flows were also accompanied

by a dilute phase indicated by units composed of fine-textured, matrix-supported, cross-laminated and lapilli-bearing tephra layers (e.g., PDC-7 or thin lenses between PDC-1 and PDC-2); units that are diagnostic of traction-dominated regimes (e.g., Branney and Kookelar, 2002) during stepwise aggradation (Sulpizio et al., 2014). Passage of the PDCs over the 20-m high waterfall at the head of the Tepu study area may have contributed to extreme turbulence, possibly accentuating the thickness of the dilute, ash-cloud surge component of the PDCs for hundreds of meters down the valley. Patterns of toppled vegetation on the valley wall suggest that these ash cloud surges super-elevated and reached as high as 62 m above the valley floor as they went around bends in the valley topography. This type of PDC behavior has been observed in other volcanic eruptions and has caused scorched zones of dead foliage in the flanks of gullies (e.g., Romero et al., 2017). Both the concentrated and diluted PDCs

have been also recognized by Macorps (2021) in the Calbuco 2015 deposits.

To estimate the velocity during the emplacement of the PDCs, we used a steady video from a survillance camera at Osorno volcano (https://youtu. be/53a 4RQC f0), which shows the beginning of the eruption and the PDCs sourced from ~800 m above the crater, descending down the Tepu valley. Due to Calbuco's north flank morphology, which corresponds to a horseshoe scar infilled by a young post-collapse composite edifice (Sellés and Moreno, 2011), the PDCs were initially unconfined until encountering the valleys downstream, becaming channelized flows. We observe that the first PDC (18:06:36 local time) travelled about 3,620 m in 98 s, thus its average velocity was  $\sim 37 \text{ m s}^{-1}$  (133 km h<sup>-1</sup>). Also, using the super-elevated PDC (h=62 m) in the Tepu (site distant 5,136 m dowstream from the crater, 488 m a.s.l. elevation), with a flow height loss (h) of 2,326 m, we can estimate the flow friction loss and velocity (Eqn. 1 and 2; Naranjo and Francis, 1987):

$$F = \left[1 - \left(\frac{h}{H}\right)^{0.5}\right] \quad (1)$$

$$v = 10 \cdot \sqrt{\frac{2 \cdot g \cdot h}{100 - F}} \quad (2)$$

We obtain for the first PDC a flow friction loss of 0.84 and velocity of 35 m s<sup>-1</sup> (126 km h<sup>-1</sup>), roughly equal to what is retrieved from the video footage. Comparatively, Macorps (2021) estimated velocities of 5.2 to 10.5 m s<sup>-1</sup> for the Blanco-Este and Frío PDCs, respectively, and 3-7 m s<sup>-1</sup> for the Blanco Sur River. According to Lube *et al.* (2011), higher channel sinuosity has potential for flow acceleration in outer bends, producing flow avulsion, mainly as overflow. On the other hand, Molle et al. (2012) studied the 8 January 2010 PDCs of Sufrière Hills volcano, and observed flow front deceleration due to high degrees of valley sinuosity. The higher sinuosity of the Tepu river valley could also explain the production of dilute PDC facies in the outer rims of the valley as consequence of overflow, although the estimated flow velocities are higher in the Tepu compared to the Blanco-Este and Frío. We suggest the valley slope (higher in the Tepu), combined with the channel width (narrower in the Tepu) were the main factors to control this behaviour, despite channel sinuosity.

## 4.2. Alluvial processes following the eruption

Our observations support the interpretation that the lahars described in this study occurred after the eruption, and thus represent lahars triggered by mild precipitation events rather than lahars triggered by direct melting of snow and glaciers from the summit of the volcano, which were not studied in this paper and their outcrops are not included in the stratigraphic sections containing the PDC deposits. In this sense, the precipitation events in the four weeks leading up to the eruption wetted the landscape somewhat, but low precipitation in the first few weeks after the eruption (~300 mm) delayed erosion of the new deposits (Fig. 6). No single, major precipitation event in the post-eruption record appears to have abruptly triggered channel incision, and various lines of evidence document fluvial erosion of the 2015 deposits proceeding progressively over months and further erosion occurring over subsequent years. For example, 1,500 mm of precipitation fell between 23 April and 1 August 2015, supporting fumaroles and erosion. By January 2018, sections of the Tepu and Frío channels had reoccupied their pre-eruption channels and streambanks, which are armored by large boulders, so the pace of sediment mobilization and geomorphic change was greatly reduced.

#### 4.3. PDC effects on vegetation

Interactions of volcanic processes and vegetation are rather well-known for many volcanic processes (e.g., Crisafulli et al., 2015; Swanson and Crisafulli, 2018), but little is known on the effect of PDCs. In the Tepu study area, PDCs left abundant evidence of many types of interactions with forest vegetation, so we are able to examine these from various perspectives. Few trees existed in the Frío valley before the eruption, probably because of disturbance during the 1961 eruption, and very few trees buried by PDC deposits have been exposed by erosion. Our charcoal data representing emplacement temperatures of 400-550 °C is consistent with recent data by Schito et al. (2022) at the Frío River, with temperatures from 408 to 566 °C measured in charcoal of Fitzroya Cupressoides at 4-5 km from the vent. Therefore, our analysis of PDC-forest interactions is restricted to the Tepu area where PDCs encountered extensive young forest on the wide valley floor, which probably regenerated after the 1961 eruption (Zingaretti et al., 2023).

Along the Tepu valley, ground-hugging PDCs tipped over smaller stems and left some larger trees standing in more protected areas at the margins and at the distal end of the deposits where flows were thin, reflecting both lateral and down-valley gradients in disturbance intensity. Trees smaller than ~10 cm DBH were bent over, but remained rooted and the tips of the remaining part of their stems were charred and with tops removed in most cases. Greater thickness of PDC deposits resulted in a greater tendency to have their tops fallen and a greater tendency for burning wood at the top of the deposit. Apparently, combustion could occur at the point where the tree stem emerged from the deposits (Fig. 8D), where the deposits were thick enough to supply the necessary heat and oxygen was available in the ambient air. The buried wood could be charred, but it did not ignite, because of limited oxygen supply within the deposits. The preferential fall of tree tops in the down-valley direction suggests that the PDCs may have had sufficient force to tip the trees slightly, predisposing them to fall in that direction (e.g., Figs. 8D and 11). The timing of fall of the tree tops relative to fluvial erosion of the PDC deposits is however uncertain.

Patterns of heat damage to detrital wood pieces and rooted trees provide evidence concerning emplacement and cooling of PDC deposits. Rooted trees exhibit increased heat damage to wood (e.g., discoloration, intensity of charring, radial fracturing of the stem) from the pre-eruption ground surface upward over a meter into the deposit. This gradient appears in cross-sections of tree stems (Fig. 9B) and exterior patterns of charring on upright trees. We did not document any heterogeneous thermal effect related to flow direction (e.g., leeward vs windward). The results obtained by Ricci et al. (2022) are in well agreement with our observations, indicating that the charcoal at the bottom of the deposit was produced by temperatures of 405 °C, whereas the top was exposed to up to 520 °C. This pattern can be explained by greater water availability near the preeruption soil or rapid water delivery to the base of the deposit soon after the formation of small watersheds, creating a water table in the base of the deposits (Fig. 11). However, these hypotheses need to be properly addressed with both laboratory and experimental data to provide a convincing explanation. Detrital wood throughout the PDC deposits appears to be completely

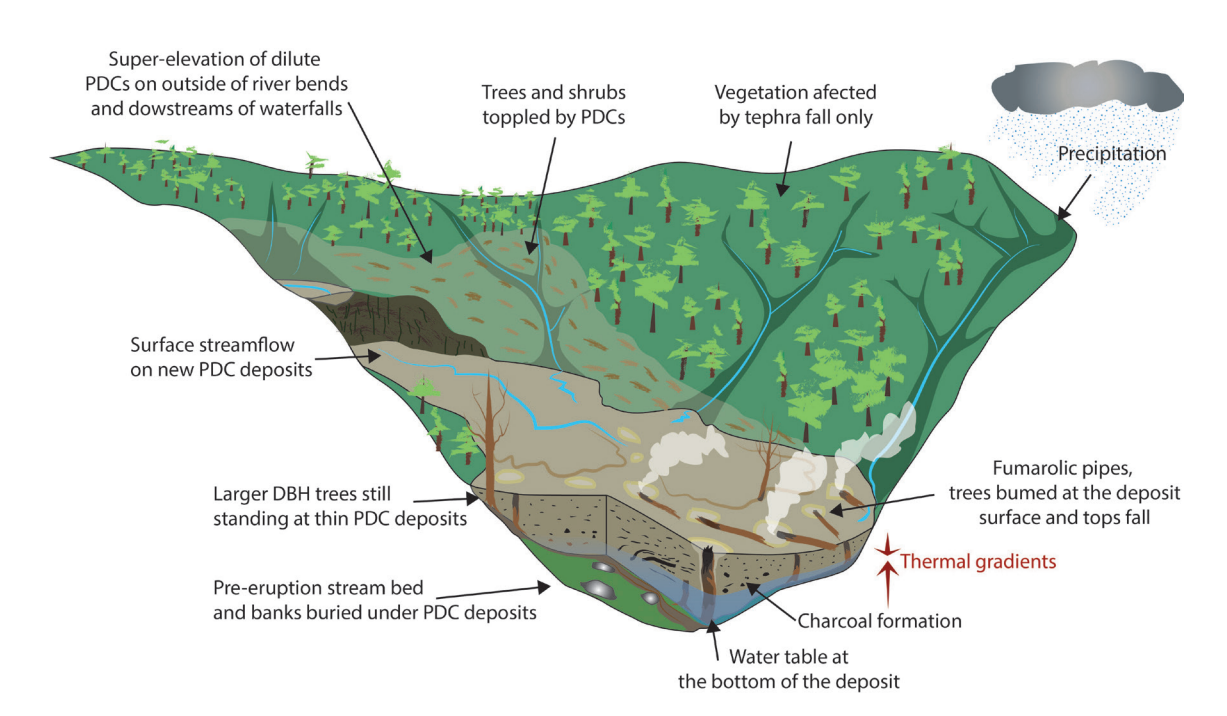


FIG. 11. Cartoon summarizing the PDC-forest interaction at the Tepu River bed (not to scale). We propose that the thermal gradients observed are explained by the early formation of a water table at the bottom of the deposit.

converted to charcoal (Fig. 9C). The small size of transported pieces may have facilitated their rapid desiccation and conversion to charcoal, possibly explaining the close juxtaposition of fully charred detrital wood fragment with the larger diameter upright tree stems that experienced less heat damage (Fig. 9D). Heating damage to the partially buried trees continued after PDC emplacement, including during the period of fumarole activity. The variability in the charring patterns observed is relevant for physical interpretations of volcaniclastic deposits and should be taken into account in future studies.

Some tree tops are now located on surfaces eroded by fluvial action (Supplementary Fig. 1), and these tops have not experienced significant transport or removal of limbs, suggesting they may have fallen after the erosion. This possibility is confirmed by the presence of sub-rounded cobbles of scoria lodged in the tree limbs, which appear to have been emplaced during bedload transport in the period of erosion of the PDC deposits (Supplementary Fig. 1). The phenomenon of fallen tops on fluvially eroded PDC deposits was also observed in the Blanco-Chaitén River valley after the 2008 eruption of Chaitén volcano (Fig. 16 in Swanson *et al.*, 2013).

Dilute PDCs produced defoliated, standing, and fallen trees and shrubs on the valley wall pointing in the down-valley direction (Fig. 8F and G). We infer this damage to foliage was the result of scorching, as observed in the case of other sites of dilute PDC movement into forests, such as on the north flank of Chaitén in its 2008 eruption (Swanson *et al.*, 2013).

To elucidate the forces involved in the toppling the trees, here we attempt to determine the dynamic pressures involved. First, we solve the particle volume concentration in the flow ( $C_{avg}$ ; Eqn. 3):

$$C_{avg} = \frac{E}{100 \cdot h_c} \cdot \frac{\left(t_0 - t_f\right)}{lnt_0 - lnt_f} \ (3)$$

where E is the volumetric void ratio (nominal value of 0.7),  $h_c$  is the depth of the flow in m (in this case, 50 m),  $t_0$  is the thickess of the deposit at its distal limit (here considered 10 cm) and  $t_f$  is the deposit thickness at a specific site. In this case, we chose the site where tree toppling is observed and the flow deposit is 40 cm depth. Consequently,  $C_{avg}$  is  $3.03 \times 10^{-3}$ . Then, the average flow density ( $\rho_{avg}$ ) is obtained from Clarke and Voight (2000) (Eqn. 4):

$$\rho_{avg} = C_{avg} \cdot \rho_s + (1 - C_{avg}) \cdot \rho_{gas}$$
 (4)

where  $\rho_s$  is the average density of solid particles and  $\rho_{gas}$  is the gas density. While the Tepu PDCs average 75% high-density scoria, 17% low-density scoria and 8% lithics, the Río Blanco-Este and Frío contain 44% high-density scoria, 45% low-density scoria and 11% lithics on average. Using the clast densities reported by Romero *et al.* (2016) for these components, we estimate for the Tepu and Frío in 1,557 kg m<sup>-3</sup> and 1,318 kg m<sup>-3</sup>, respectively. (It is relevant to mention that only the dilute and turbulent parts can be modeled by these fluid dynamics, while the ground-hugging concentrated PDC is governed by granular flow laws; *e.g.*, Bursik *et al.*, 2005.)

Then,  $\rho_{avg}$  is 5.0-5.7 kg m<sup>-3</sup>. Using a mean velocity of 36 m s<sup>-1</sup>, the dynamic pressures ( $P_{dyn}$ ) are estimated using Eqn. 5:

$$P_{dyn} = \frac{1}{2} \rho_{avg} v^2 \tag{5}$$

which range from 3.2 to 3.7 kPa. Another way to obtain the dynamic pressure is based on the scorched trees' dimensions (Eqn. 6):

$$P_{dyn} = \frac{M}{r_t l_t^2 C_d}$$
 (6)

For the Calbuco case, the scorched trees have conical shape with 0.4 m basal diameter (DBH) and a mean length of 13 m  $(l_{.})$ , thus a volume of 1.3 m<sup>3</sup>. Considering a density of 650 kg m<sup>-3</sup> (see Major *et al.*, 2013), their average weights were nearly 845 kg. Then, the force required to uproot these trees is 100-200 times their weight, thus implying a moment (M) of  $8.5-17 \times 10^4$  Nm. With an aerodynamic drag coefficient C<sub>4</sub> assumed to be 1.1 (Guinn et al., 2022), we estimate the minimum  $P_{dvn}$  necessary to topple these trees was roughly 1.5-3.0 kPa. This range of  $P_{dvn}$  is slightly lower compared to that obtained from the flow density and velocity; consequently, the latter can be considered a maximum value. Comparatively, the Chaitén 2008 PDCs had flow densities of 2-3 kg m<sup>-3</sup> and dynamic pressures from 2 to 4 kPa (Major et al., 2013). In part, this consistency is explained by a similar tree asamblage in Calbuco to that observed in Chaitén (e.g., Hintz et al., 2021). On the other hand, dynamic pressures observed in blowndown trees at Mount St. Helens (USA), Merapi (Indonesia) and Maungataketake (New Zealand) volcanoes range from 10 to 40 kPa (Clarke and Voight, 2000; Jenkins et al., 2013; Brand et al., 2014; Guinn et al., 2022), however these mostly correspond to blast events. In contrast, Macorps (2021) estimated dynamic pressures of 18.6 to 74.5 kPa for the Calbuco PDCs.

### 4.4. Extent of vegetation disturbance

Past studies on the effects of volcanic processes on biota have highlighted the value of considering the consequences of ecological disturbance mechanisms (e.g., heating, impact force, abrasion, burial) rather than focusing only on the type of geophysical process (e.g., PDC, tephra fall, lahar) (Swanson et al., 2013; Crisafulli et al., 2015; Swanson and Crisafulli, 2018). Each disturbance type involves one or more mechanisms that are sensed by plants and animals. The PDCs at Calbuco involved the principle mechanisms of impact force, abrasion, burial, and heat due to their sedimentology and fluid mechanics. Of this suite of disturbance mechanisms, heat and impact force appear to have been the dominant and immediate causes of biota mortality in the Tepu study site, which is at the lower end of the PDC run out path where impact force was decreasing (Fig. 11).

The combination of heat, impact force, and possibly flow velocity, was sufficient to bend over small trees, but some larger diameter trees remained standing. Impact force of the PDCs in the study area was insufficient to uproot trees, as indicated by lack of root pits where trees had been plucked from the soil, paucity of trees with attached root systems within the PDC deposits, and absence of an accumulation of transported whole trees at the toe of the deposit. Despite these observations of low-impact force of the PDCs at the lower end of their run out paths, we expect the impact force to have been much greater higher in the valley, i.e., in the middle and upper sections of the flows, as indicated by the presence of lithic breccias and high-density metric bombs in these deposits (e.g., Janda et al., 1981; Glicken, 1998). In consequence, the estimates obtained by Macorps (2021) can be more realistic of such conditions. Heating from partial burial of stems within PDC deposits appears to have killed all affected trees immediately, even where the deposits were only 20 cm thick, which seems consistent with the hot deposit temperatures indicated in this investigation.

Abrasion by PDCs imposed some damage to upright and tipped stems on their upstream sides, as indicated by asymmetrical removal of bark and wood, but in some sites subsequent bedload transport of cobbles during fluvial erosion appears to have caused more abrasion than the low-density, gascharged PDCs, as indicated by the bark present on upright trees still partially buried in PDC deposits. These lower-temperature impacts contradict recent findings in Herculaneum during the 79 CE eruption of Vesuvius, where dilute PDCs left a lethal thermal overprint on the residents (Pensa et al., 2023). Despite the differences leading to heterogeneous impacts produced by the Calbuco 2015 PDCs compared to those in Vesuvius require an in-deep investigation, one possible explanation is related to ash-cloud decoupling. In this respect, the passage of the ground hugging PDCs over the 20-m high waterfall may have facilitated instantaneous air entrainment -increasing turbulence- and hence facilitating rapid cooling of the dilute PDCs.

## 5. Conclusions

The 22 and 23 April 2015 eruption of Calbuco volcano produced pyroclastic density currents (PDCs) which affected the valleys of Tepu and Frío rivers in the north flank of the volcano. These PDCs travelled as far as 7-8 km from the crater. The Tepu PDCs were the first to occur, mainly during the first pulse on the 22 April 2015, while most of the Frío PDCs occurred on 23 April 2015 during the second pulse. All the PDC deposits develop small-scale features, such as stepwise aggradation and the existence of multiple beds, and show evidence of both concentrated flows and diluted accompanying phases.

Here we recognized different mechanisms of vegetation disturbance related to PDCs, such as heating, abrasion, burial, and impact force. Concentrated PDCs had a much more profound impact on vegetation (e.g., toppling, charring, killing all stems that had deposits at their base) than dilute PDCs, which bent over small trees and shrubs and scorched foliage, but advection of heat to tree stems was so brief and deposits on the ground so thin that sprouting was possible for some species.

Further erosion and river incision affecting the 2015 PDC deposits, months-to-years after the eruption, imprints additional geomorphic changes that involve the transport of sediment to the lower depositional areas in the Blanco-Este River and Llanquihue Lake, thus suggesting long-term impacts related to volcanic eruptions.

This study highlights the importance of visiting field sites within days of an eruption and revisiting frequently as key events unfold, especially fluvial erosion which reveals fresh exposures of the new deposits and their interactions with vegetation while at the same time removes parts of that record. A thorough, interdisciplinary approach brings the benefit of information provided by the record of damage to vegetation due to volcanic processes and their contribution to hazards.

### Acknowledgments

J. Romero acknowledges University of Atacama for the partial support of field work at Calbuco during the 2017 Cities on Volcanoes conference in Puerto Varas. We thank P. Saumann and B. Corrales of Parque Valle los Ulmos in Ensenada, Chile, for many forms of support, information, and insights. We thank A. Ziller for access to Blanco-Este River. F. Swanson and J. Jones thank Universidad Austral de Chile, Center and Climate and Resilience Research (CR<sup>2</sup>) for travel support in 2016 and A. Iroume for support of FS through a Conicyt grant. This work was supported in part by a MEC80170010 Conicyt grant. M. Mella (Sernageomin) shared helpful comments and interpretations in the field. The reviews provided by T.C. Pierson and D. Huntzinger on an early version of this manuscript are appreciated and contributed to improve this contribution. Additionally, we are grateful with the reviews of W. Báez, two anonymous reviewers, and the editorial handling of D. Bertin for their insightful suggestions. A. Becerra and G. Cifuentes provided useful photographs of the PDCs during the eruption. We thank forest science professors K. Kavanagh, B. Lachenbruch, and M. Milota (Oregon State University) and A. Rolleri (U. Austral de Chile) for consultations concerning responses of wood and water content to extreme heat. Supplementary material is stored at https://doi.org/10.6084/m9.figshare.c.6757212.v1.

#### References

- Arzilli, F.; Morgavi, D.; Petrelli, M.; Polacci, M.; Burton,
  M.; Di Genova, D.; Spina, L.; La Spina, G.; Hartley,
  M.; Romero, J.E.; Fellowes, J.; Díaz-Alvarado, J.;
  Perugini, D. 2019. The unexpected explosive sub-Plinian eruption of Calbuco volcano (22-23 April 2015; southern Chile): Triggering mechanism implications. Journal of Volcanology and Geothermal Research 378: 35-50.
- Ascough, P.L.; Bird, M.I.; Scott, A.C.; Collinson, M.E.; Cohen-Ofri, I.; Snape, C.E.; Le Manquais, K. 2010. Charcoal reflectance measurements: implications for structural characterization and assessment of diagenetic

- alteration. Journal of Archaeological Science 37: 1590-1599.
- Bertin, D.; Amigo, Á.; Mella, M.; Astudillo, V.; Bertin, L.;
  Bucchi, F. 2015. Erupción del volcán Calbuco 2015:
  Estratigrafía eruptiva y volumen involucrado. *In*Congreso Geológico Chileno, No. 14, Actas: 132-135. La Serena.
- Bown, F. 2004. Cambios climáticos en la Región de Los Lagos y respuestas recientes del Glaciar Casa Pangue (41°08'S). Tesis de Magíster en Geografía, Universidad de Chile: 114 p.
- Brand, B.D.; Gravley, D.M.; Clarke, A.B.; Lindsay, J.M.; Bloomberg, S.H.; Agustin-Flores, J.; Németh, K. 2014. A combined field and numerical approach to understanding dilute pyroclastic density current dynamics and hazard potential: Auckland volcanic field, New Zealand. Journal of Volcanology and Geothermal Research 276: 215-232.
- Branney, M.J.; Kokelaar, P. 2002. Pyroclastic Density Currents and the Sedimentation of Ignimbrites. Geological Society, Memoir: 27: 152 p. London.
- Bursik, M.; Patra, A.; Pitman, E.B.; Nichita, C.; Macias, J.L.; Saucedo, R.; Girina, O. 2005. Advances in studies of dense volcanic granular flows. Reports on Progress in Physics 68 (2): 271 p.
- Caricchi, C.; Vona, A.; Corrado, S.; Giordano, G.; Romano, C. 2014. 79 AD Vesuvius PDC deposit's temperatures inferred from optical analysis on woods charred *in-situ* in the Villa dei Papiri at Herculaneum (Italy). Journal of Volcanology and Geothermal Research 289: 14-25.
- Castruccio, A.; Clavero, J.; Rivera, A. 2010. Comparative study of lahars generated by the 1961 and 1971 eruptions of Calbuco and Villarrica volcanoes, Southern Andes of Chile. Journal of Volcanology and Geothermal Research 190: 297-311.
- Castruccio, A.; Clavero, J.; Segura, A.; Samaniego, P.; Roche, O.; Le Pennec, J.L.; Droguett, B. 2016. Eruptive parameters and dynamics of the April 2015 sub-Plinian eruptions of Calbuco volcano (southern Chile). Bulletin of Volcanology 78 (9): 62. doi: https://doi.org/10.1007/s00445-016-1058-8
- Cioni, R.; Furioli, L.; Lanza, R.; Zanella, E. 2004. Temperatures of the A.D. 79 pyroclastic density current deposits (Vesuvius, Italy). Journal of Geophysical Research 109 (B02207). doi: https://doi.org/10.1029/2002JB002251
- Clarke, A.B.; Voight, B. 2000. Pyroclastic current dynamic pressure from aerodynamics of tree or pole blow-down. Journal of Volcanology and Geothermal Research 100: 395-412.

- Crisafulli, C.M.; Swanson, F.J.; Halvorson, J.J.; Clarkson, B.D. 2015. Volcano ecology: disturbance characteristics and assembly of biological communities. *In* The encyclopedia of volcanoes (Sigurdsson, H.; Houghton, B.; McNutt, S.; Rymer, H.; Stix, J.; editors) Elsevier: 1265-1284. Amsterdam.
- DGA. 1995. Manual de cálculo de crecidas y caudales mínimos en cuencas sin información fluviométrica.
   Ministerio de Obras Públicas, Dirección General de Aguas: 147 p. Santiago.
- Furukawa, K.; Uno, K.; Shinmura, T.; Miyoshi, M.; Kanamaru, T.; Inokuchi, H. 2014. Origin and mode of emplacement of lithic-rich breccias at Aso Volcano, Japan: Geological, paleomagnetic, and petrological reconstruction. Journal of Volcanology and Geothermal Research 276: 22-31.
- Giggenbach, W.F. 1987. Redox processes governing the chemistry of fumarolic gas discharges from White Island, New Zealand. Applied Geochemistry 2 (2): 143-161.
- Giggenbach, W.F. 1996. Chemical composition of volcanic gases. *In* Monitoring and mitigation of volcano hazards (Scarpa, R.; Tilling, R.I.; editors). Springer: 221-256. Berlin.
- Glicken, H. 1998. Rockslide-debris avalanche of May 18, 1980, Mount St. Helens volcano, Washington. Bulletin of the Geological Survey of Japan 49: 55-106.
- Global Volcanism Program. 2013. Calbuco (358020). *In* Volcanoes of the World v. 4.8.6. (Venzke, E.; editor). Smithsonian Institution. Downloaded 28 Feb 2020.
- Guinn, N.K.; Gardner, J.E.; Helper, M.A. 2022. Dynamic pressure evolution within the 18 May 1980 Mount St. Helens pyroclastic density current: evidence from tree damage. Bulletin of Volcanology 84: 38 p.
- Hernández, V. 2018. Efecto de erupciones volcánicas sobre los patrones de establecimiento y Crecimiento de Nothofagus dombeyi y Drimys winteri. Master thesis (Unpublished), Universidad Austral de Chile: 37 p.
- Hintz, L.; Fischer, D.; Ferrari, N.; Crisafulli, C. 2021. Vegetation dynamics under residual large trees following a volcanic eruption in a Valdivian temperate rainforest. Plant Ecology 222: 915-931.
- Hudspith, V.A.; Scott, A.C.; Wilson, C.J.N.; Collinson, M.E. 2010. Charring of woods by volcanic processes: An example from the Taupo ignimbrite, New Zealand. Paleogeography, Paleoclimatology, Paleoecology 291: 40-51.
- Janda, R.J.; Scott, K.M.; Nolan, K.M.; Martinson, H.A. 1981. Lahar movement, effects, and deposits. *In* The 1980 Eruptions of Mount St. Helens, Washington (Lipman, P.W.; Mullineaux, D.R.; editors). U.S.

- Geological Survey, Professional Paper 1250: 461-478. Washington.
- Jenkins, S.; Komorowski, J.C.; Baxter, P.J.; Spence, R.; Picquout, A.; Lavigne, F.; Surono. 2013. The Merapi 2010 eruption: an interdisciplinary impact assessment methodology for studying pyroclastic density current dynamics. Journal of Volcanology and Geothermal Research 261: 316-329.
- Jones, R.J. 2016. Initiation of rain-triggered lahars. Ph.D. Thesis (Unpublished). University of Leeds: 271 p.
- Klohn, E. 1963. The February 1961 eruption of Calbuco Volcano. Bulletin of the Seismological Society of America 53 (6): 1435-1436.
- Lube, G.; Cronin, S.J.; Thouret, J.C.; Surono, S. 2011.
  Kinematic characteristics of pyroclastic density currents at Merapi and controls on their avulsion from natural and engineered channels. Geological Society of America Bulletin 123 (5-6): 1127-1140.
- Macorps, E. 2021. Field and Remote Sensing Analysis of the 2015 Pyroclastic Density Currents at Colima (Mexico) and Calbuco (Chile) Volcanoes: Implications for Hazard Assessment and Crisis Managemen. Doctoral Dissertation, University of South Florida: 340 p.
- Major, J.J.; Pierson, T.C.; Hoblitt, R.P.; Moreno, H. 2013. Pyroclastic density currents associated with the 2008-2009 eruption of Chaitén Volcano (Chile): Forest disturbances, deposits, and dynamics. Andean Geology 40 (2) 324-358. doi: http://dx.doi.org/10.5027/andgeoV40n2-a09
- Major, J.J.; Bertin, D.; Pierson, T.C.; Amigo, Á.; Iroumé, A.; Ulloa, H.; Castro, J. 2016. Extraordinary sediment delivery and rapid geomorphic response following the 2008-2009 eruption of Chaitén Volcano, Chile. Water Resources Research 52 (7): 5075-5094.
- Mella, M.; Moreno, H.; Vergés, A.; Quiroz, D.; Bertin, L.; Basualto, D.; Bertin, D.; Garrido, N. 2015. Productos volcánicos, impactos y respuestra a la emergencia del ciclo eruptivo abril-mayo (2015) del Volcán Calbuco. *In* Congreso Geologico Chileno, No. 14, Actas: 98-101. La Serena.
- Molle, A.; Ogburn, S.E.; Calder, E.S.; Roche, O.; Harris, A.J. 2012. Dynamic observations of the 8 January 2010 pyroclastic flow from the Soufriere Hills Volcano, Montserrat ascertained by high-definition and FLIR video analysis, as well as geometric analysis of the DEM. *In* AGU Fall Meeting, Abstracts: V52C-04.
- Moreno, H.; Naranjo, J.A.; Clavero, J. 2006. Generación de lahares calientes en el volcán Calbuco, Andes del sur de Chile (41,3°S). *In* Congreso Geológico Chileno, No. 11, Actas: 512-513. Antofagasta.

- Morgado, E.; Morgan, D.J.; Harvey, J.; Parada, M.A.; Castruccio, A.; Brahm, R.; Gutiérrez, F.; Georgiev, B.; Hammond, S.J. 2019. Localised heating and intensive magmatic conditions prior to the 22-23 April 2015 Calbuco volcano eruption (Southern Chile). Bulletin of Volcanology 81: 24 p.
- Naranjo, J.A.; Francis, P. 1987. High velocity debris avalanche at Lastarria volcano in the north Chilean Andes. Bulletin of Volcanology 49 (2): 509-514
- Pensa, A.; Capra, L.; Giordano, G.; Corrado, S. 2018. Emplacement temperature estimation of the 2015 dome collapse of Volcán de Colima as key proxy for flow dynamics of confined and unconfined pyroclastic density currents. Journal of Volcanology and Geothermal Research 357: 321-338.
- Pensa, A.; Capra, L.; Giordano, G. 2019. Ash clouds temperature estimation. Implication on dilute and concentrated PDCs coupling and topography confinement. Scientific Reports 9 (1): 5657. doi: https://doi.org/10.1038/s41598-019-42035-x
- Pensa, A.; Giordano, G.; Corrado, S.; Petrone, P.P. 2023.

  A new hazard scenario at Vesuvius: deadly thermal impact of detached ash cloud surges in 79CE at Herculaneum. Scientific Reports 13 (1): 5622. doi: https://doi.org/10.1038/s41598-023-32623-3
- Pierson, T.C.; Major, J.J.; Amigo, Á.; Moreno, H. 2013. Acute sedimentation response to rainfall following the explosive phase of the 2008-2009 eruption of Chaitén volcano, Chile. Bulletin of Volcanology 75 (5): 723.
- Reckziegel, F.; Bustos, E.; Mingari, L.; Báez, W.; Villarosa, G.; Folch, A.; Collini, E.; Viramonte, J.; Romero, J.; Osores, S. 2016. Forecasting volcanic ash dispersal and coeval resuspension during the April-May 2015 Calbuco eruption. Journal of Volcanology and Geothermal Research 321: 44-57.
- Ricci, L.; Pensa, A.; Morgavi, D.; Ariano, A.; Romero, J.; Giordano, G.; Frondini, F. 2022. Emplacement temperature estimation of the 2015 Calbuco pyroclastic density currents (PDCs) using charcoal reflectance (Ro%) method: Preliminary results. *In* Conferenza A. Rittmann, No. 5. Catania.
- Risica, G.; Rosi, M.; Pistolesi, M.; Speranza, F.; Branney, M.J. 2022. Deposit-Derived Block-and-Ash Flows: The Hazard Posed by Perched Temporary Tephra Accumulations on Volcanoes; 2018 Fuego Disaster, Guatemala. Journal of Geophysical Research: Solid Earth 127 (6): doi: https://doi.org/10.1029/2021JB023699.
- Romero, J.E.; Morgavi, D.; Arzilli, F.; Daga, R.; Caselli, A.; Reckziegel, F.; Viramonte, J.; Díaz-Alvarado, J.; Polacci, M.; Burton, M.; Perugini, D. 2016. Eruption

- dynamics of the 22-23 April 2015 Calbuco Volcano (southern Chile): Analyses of tephra fall deposits. Journal of Volcanology and Geothermal Research 317: 15-29.
- Romero, J.E.; Douillet, G.A.; Vallejo Vargas, S.; Bustillos,
  J.; Troncoso, L.; Díaz-Alvarado, J.; Ramón, P. 2017.
  Dynamics and style transition of a moderate, Vulcanian-driven eruption at Tungurahua (Ecuador) in February
  2014: pyroclastic deposits and hazard considerations.
  Solid Earth 8: 697-719.
- Romero, J.E.; Alloway, B.V.; Gutiérrez, R.; Bertin, D.; Castruccio, A.; Villarosa, G.; Schipper, I., Guevara, A.; Bustillos, J.; Pisello, A.; Daga, R.; Montiel, M.; Gleeman, E.; González, M.; Morgavi, D.; Riveiro Guevara, S.; Mella, M. 2021. Centennial-scale eruptive diversity at Volcán Calbuco (41.3° S; Northwest Patagonia) deduced from historic tephra cover-bed and dendrochronologic archives. Journal of Volcanology and Geothermal Research 417: doi: https://doi.org/10.1016/j.jvolgeores.2021.107281
- Sarricolea, P.; Herrera-Ossandón, M.; Meseguer-Ruiz, O. 2017. Climatic regionalisation of continental Chile. Journal of Maps 13 (2): 66-73.
- Schito, A.; Pensa, A.; Romano, C.; Corrado, S.; Vona,
  A.; Trolese, M.; Morgavi, D.; Giordano, G. 2022.
  Calibrating Carbonization Temperatures of Wood
  Fragments Embedded within Pyroclastic Density
  Currents through Raman Spectroscopy. Minerals, 12
  (2): 203. doi: https://doi.org/10.3390/min12020203
- Scott, A.C.; Jones, T.P. 1991. Microscopical observations of recent and fossil charcoal. Microscopy and Analysis 24: 13-15.
- Scott, A.C.; Glasspool, I.J. 2005. Charcoal reflectance as a proxy for the emplacement temperature of pyroclastic flow deposits. Geology 33: 589-592.
- Scott, A.C.; Glasspool, I.J. 2007. Observations and experiments on the origin and formation of inertinite group macerals. International Journal of Coal Geology 70: 43-66.
- Scott, A.C.; Sparks, R.S.J.; Bull, I.D.; Knicker, H.; Evershed, R.P. 2008. Temperature proxy data and their significance for the understanding of pyrpclastic density currents. Geology 36: 143-146.
- Sellés, D.; Moreno, H. 2011. Geología del Volcano Calbuco, región de Los Lagos. Servicio Nacional de Geología y Minería, Carta Geológica de Chile, Serie Geologia Basica 130: 38 p., 1 mapa escala 1:50.000.
- Sulpizio, R.; Mele, D.; Dellino, P.; La Volpe, L. 2007. Deposits and physical properties of pyroclastic density currents during complex Subplinian eruptions: the AD 472 (Pollena) eruption of Somma-Vesuvius, Italy. Sedimentology 54: 607-635.

- Sulpizio, R.; Dellino, P.; Doronzo, D.M.; Sarocchi, D. 2014. Pyroclastic density currents: state of the art and perspectives. Journal of Volcanology and Geothermal Research 283: 36-65.
- Swanson, F.J.; Crisafulli, C.M. 2018. Volcano ecology: state of the field and contributions of Mount St. Helens research. *In* Ecological responses at Mount St. Helens: revisited 35 years after the 1980 eruption (Crisafulli, C.M.; Dale, V.H.; editors). Springer: 305-323. New York.
- Swanson, F.J.; Jones, J.A.; Crisafulli, C.M.; Lara. A. 2013. Effects of volcanic and hydrologic processes on forest vegetation: Chaiten volcano, Chile. Andean Geology, 40 (2): 359-391. doi: http://dx.doi.org/10.5027/ andgeoV40n2-a10
- Swanson, F.J.; Jones, J.; Crisafulli, C.; González, M.E.; Lara, A. 2016. Puyehue-Cordón Caulle eruption of 2011: tephra fall and initial forest responses in the Chilean Andes. Bosque 37 (1): 85-96. doi: https://doi. org/10.4067/S0717-92002016000100009.
- Swanson, F.J.; Gregory, S.V.; Iroume, A.; Ruiz-Villanueva, V.; Wohl, E. 2021. Reflections on the history of research on large wood in rivers. Earth Surface Processes and Landforms 46: 55-66.
- Trolese, M.; Giordano, G.; Komorowski, J.-C.; Jenkins,
  S.F.; Baxter, P.J.; Cholik, N.; Raditya, P.; Corrado, S.
  2018. Very rapid cooling of the energetic pyroclastic density currents associated with the 5 November 2010
  Merapi eruption (Indonesia). Journal of Volcanology and Geothermal Research 358: 1-12.
- Ulloa, H.; Iroumé, A.; Picco, L.; Mohr, C.H.; Mazzorana, B.; Lenzi, M.A.; Mao, L. 2016. Spatial analysis of the

- impacts of the Chaitén volcano eruption (Chile) in three fluvial systems. Journal of South American Earth Sciences 69: 213-225.
- Valdés-Pineda, R.; Pizarro, R.; García-Chevesich, P.; Valdés, J.B.; Olivares, C.; Vera, M.; Balocchi, F.; Pérez, F.; Vallejos, C.; Fuentes, R.; Abarza, A.; Helwig, B. 2014. Water governance in Chile: Availability, management and climate change. Journal of Hydrology 519: 2538-2567.
- Vallance, J.W.; Iverson, R.M. 2015. Lahars and their deposits. In The encyclopedia of volcanoes (Sigurdsson, H.; McNutt., S.; Rymer, H.; Stix, J.; editors). Academic Press: 649-664 London.
- Van Eaton, A.R.; Amigo, Á.; Bertin, D.; Mastin, L.G.; Giacosa, R.E.; González, J.; Valderrama, O.; Fontijn, K.; Behncke, S.A. 2016. Volcanic lightning and plume behavior reveal evolving hazards during the April 2015 eruption of Calbuco volcano, Chile. Geophysical Research Letters 43 (7): 3563-3571.
- Vaselli, O.; Tassi, F.; Montegrossi, G.; Capaccioni, B.; Giannini, L. 2006. Sampling and analysis of volcanic gases. Acta Vulcanologica 18(1-2): 1000-1012.
- Yasuda, Y.; Suzuki-Kamata, K. 2018. The origin of a coarse lithic breccia in the 34 ka caldera-forming Sounkyo eruption, Taisetsu volcano group, central Hokkaido, Japan. Journal of Volcanology and Geothermal Research 357: 287-305.
- Zingaretti, V.; Iroumé, A.; Llena, M.; Mazzorana, B.; Vericat, D.; Batalla, R.J. 2023. Geomorphological evolution of the Blanco Este River after recent eruptions of the Calbuco volcano, Chile. Geomorphology 427. doi: https://doi.org/10.1016/j.geomorph.2022.108570

Manuscript received: February 04, 2023; revised/accepted: July 20, 2023; available online: July 25, 2023.

## **Supplementary Material**

https://doi.org/10.6084/m9.figshare.c.6415370.v1